

1-11-2023

## Solar-light-responsive nanomaterials for the photoelectrocatalytic degradation of stubborn pollutants

Benjamin O. Orimolade

Azeez O. Idris


Seyi Philemon Akanji  
*Edith Cowan University*

Folahan A. Adekola

Shohreh Azizi

*See next page for additional authors*

Follow this and additional works at: <https://ro.ecu.edu.au/ecuworks2022-2026>

 Part of the [Nanoscience and Nanotechnology Commons](#)

---

[10.3390/coatings13010159](https://doi.org/10.3390/coatings13010159)

Orimolade, B. O., Idris, A. O., Akanji, S. P., Adekola, F. A., Azizi, S., Maaza, M., & Mamba, B. (2023). Solar-light-responsive nanomaterials for the photoelectrocatalytic degradation of stubborn pollutants. *Coatings*, 13(1), Article 159. <https://doi.org/10.3390/coatings13010159>

This Journal Article is posted at Research Online.  
<https://ro.ecu.edu.au/ecuworks2022-2026/1904>

---

## Authors

Benjamin O. Orimolade, Azeez O. Idris, Seyi Philemon Akanji, Folahan A. Adekola, Shohreh Azizi, Malik Maaza, and Bhekie Mamba

Review

# Solar-Light-Responsive Nanomaterials for the Photoelectrocatalytic Degradation of Stubborn Pollutants

Benjamin O. Orimolade <sup>1,2,\*</sup>, Azeez O. Idris <sup>3,4,\*</sup>, Seyi Philemon Akanji <sup>5</sup>, Folahan A. Adekola <sup>2</sup>, Shohreh Azizi <sup>3,4</sup>, Malik Maaza <sup>3,4</sup> and Bhekhe Mamba <sup>3,4</sup>

- <sup>1</sup> Institute for Nanotechnology and Water Sustainability (iNanoWS), College of Science, Engineering and Technology, Florida Science Campus, University of South Africa, Johannesburg 1709, South Africa
  - <sup>2</sup> Department of Industrial Chemistry, University of Ilorin, Ilorin P.O. Box 1515, Nigeria
  - <sup>3</sup> UNESCO-UNISA Africa Chair in Nanoscience and Nanotechnology College of Graduates Studies, University of South Africa, Pretoria 392, South Africa
  - <sup>4</sup> Nanosciences African Network (NANOAFNET), iThemba LABS-National Research Foundation, Somerset West 7129, South Africa
  - <sup>5</sup> Petroleum Engineering, School of Engineering, Edith Cowan University, Perth 6027, Australia
- \* Correspondence: orimobo@unisa.ac.za (B.O.O.); eadrisao@unisa.ac.za (A.O.I.)

**Abstract:** Due to the ever increasing demand for cleaner water, a remarkable focus has been on the use of nanomaterials in wastewater treatment application. Photoelectrocatalytic (PEC) degradation, an advanced oxidation process which combines light and electrical energy, has been identified as a suitable technique capable of achieving total mineralisation of recalcitrant organic pollutants in wastewater. PEC degradation is non-selective, environmentally friendly and possesses great efficiency. The efficiency of PEC degradation has been enhanced by fabricating the photoanodes on a nanoscale with distinct morphologies. These nanostructured photoanodes have been extensively used for the removal of pharmaceuticals, dyes and phenolic water from wastewater. In many cases, total degradation of the pollutants is achieved within 2 h with significant TOC removal. This review presents an overview of the remarkable success that has been recorded with the use of nanostructured photoanodes in PEC degradation in the presence of visible light. The techniques that are commonly employed to improve the solar light responsiveness of these photoanodes are well discussed. Additionally, the use of nanostructured photoanodes consisting of heterojunction in PEC degradation is also presented. It is our aim that this review will help researchers to make informed decisions regarding the use of nanomaterials in PEC water treatment.

**Keywords:** nanomaterials; organic pollutants; photoanodes; photoelectrocatalytic degradation; water treatment



**Citation:** Orimolade, B.O.; Idris, A.O.; Akanji, S.P.; Adekola, F.A.; Azizi, S.; Maaza, M.; Mamba, B. Solar-Light-Responsive Nanomaterials for the Photoelectrocatalytic Degradation of Stubborn Pollutants. *Coatings* **2023**, *13*, 159. <https://doi.org/10.3390/coatings13010159>

Academic Editor: Maria Vittoria Diamanti

Received: 13 December 2022

Revised: 31 December 2022

Accepted: 3 January 2023

Published: 11 January 2023



**Copyright:** © 2023 by the authors. Licensee MDPI, Basel, Switzerland. This article is an open access article distributed under the terms and conditions of the Creative Commons Attribution (CC BY) license (<https://creativecommons.org/licenses/by/4.0/>).

## 1. Introduction

Over the years, there has been an increase in demand for clean usable water around the globe. The major challenge facing the availability of clean water is the rise in water pollution. Many people, particularly in rural areas, do not have access to clean drinkable water. Though natural phenomena such as volcanic eruption and acid rain could cause water pollution, a larger percentage of water pollution originates from human activities [1]. There has been a tremendous increase in industrial activities which are responsible for the generation of many wastes that could eventually end up in water bodies. Several kinds of wastes including organics emanating from both industrial and household effluents have been reportedly detected in surface, underground and drinking water [2–4]. Recalcitrant organics such as pharmaceutical residues which have been classified as emerging contaminants are of major concern because of the risk associated with them. Pharmaceutical residues have been found in concentrations as high as milligrams per litre in wastewater [5].

In as much as effluents from pharmaceutical industries are the major point source of these pollutants, improper disposal of unused and expired drugs in the household also contribute to this pollution [6]. The hazardous effects of exposure to water contaminated with organics such as pharmaceuticals could be acute or chronic depending on the concentration of the pollutants in the water and the duration of exposure. For instance, a major problem is the development of strains of bacteria which are resistant to antibiotics when humans consume water contaminated with antibiotics over a period of time [7]. Aquatic lives are particularly at risk due to the contamination of water bodies with recalcitrant organics [8]. The effect of water pollution is drastic both from the economic and health viewpoint. Therefore, the focus has been on the treatment of wastewater to eliminate these pollutants [9].

The advancement in nanotechnology has led to pronounced achievements in the field of water treatments [10–12]. Nanomaterials, from both synthetic and natural sources, have found applications in different fields of water treatment. For instance, in adsorption studies, nanomaterials (nano adsorbents) from inorganic and organic substances have been extensively applied for the removal of heavy metals as well as organic pollutants [13]. This is because nano adsorbents possess a large surface area, high porosity, and large surface area to volume ratio and can be chemically regenerated [14]. Similarly, in the field of photocatalysis, much attention has been given to the preparation of metal oxide semiconductor photocatalysts on the nanoscale as well as the incorporation of nanomaterials (carbon-based) into photocatalysts [15]. This is because studies have shown that photocatalytic efficiencies of nano-scaled metal oxide semiconductors are higher due to increased photoactive surface area. Additionally, nanomaterials have found applications in water desalination [16,17].

Unfortunately, just like other conventional wastewater treatment methods, many existing water treatment techniques based on the use of nanomaterials are still not effective when it comes to the complete removal of recalcitrant organic pollutants. As evident, effluents from wastewater treatment plants have been found to still contain these recalcitrant organic pollutants such as pharmaceutical residues [18,19]. Specifically, adsorption only transfers pollutants from one media to the other which results in the formation of secondary pollutants. Similarly, incomplete degradation of organics is a common occurrence in photocatalysis due to several factors. One such factor is that photocatalysts are prone to the problem of recombination of photogenerated charge carriers which greatly reduces their photocatalytic efficiencies [20]. Therefore, the focus has been given to techniques that are capable of the complete degradation of organic pollutants in water.

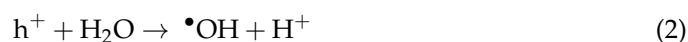
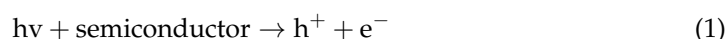
Photoelectrocatalysis (PEC) has been identified as a suitable technique capable of the complete removal of organic pollutants from wastewater. As an advanced oxidation technique, in PEC degradation hydroxyl radicals are used to non-selectively mineralise organics in the water to carbon dioxide and water [21]. Metal oxide semiconductors are used as anodic material in PEC degradation and the removal efficiency of organics largely depends on the performance of the metal oxide semiconductors. As observed in photocatalysis, the major challenge of metal oxide semiconductors is the problem of spontaneous recombination of photogenerated electron-hole pairs and this also impedes the performance of anodic materials in PEC water treatment [22,23]. In as much as the applied potential in PEC helps to greatly suppress this problem in PEC degradation by driving away electrons from the anode, several other approaches are being used to further enhance the photocatalytic efficiencies of the anode [24]. A common method is a morphology and structural manipulation of anodic materials which are usually achieved by preparing the anodic materials on a nanoscale. Additionally, since PEC depends on light irradiation, the cost associated with its operation is greatly reduced by harnessing solar energy as a source of irradiation. Numerous organics including pharmaceuticals, phenols and dyes have been successfully degraded using anodes made of solar-responsive nanomaterials. It is necessary to present researchers with relative information on the use of nanomaterials as efficient anodic materials for the removal of organics. Therefore, the scope of this review is to discuss the progress in the use of nanomaterials as efficient photoanodes. The fundamental

principles of PEC degradation are presented. Various methods of improving the solar responsiveness of metal oxide semiconductor nanomaterials are well emphasized.

### 1.1. Fundamentals of Photoelectrocatalytic Degradation

Photoelectrocatalytic (PEC) degradation (or photoelectrochemical oxidation) belongs to the group of electrochemical advanced oxidation processes (EAOP) for wastewater treatment applications which use strong hydroxyl radicals to eliminate organics. In PEC degradation, the oxidation of organics is achieved through the combined action of two processes: photocatalysis and electrochemical oxidation. As an EAOP system, PEC degradation has some outstanding advantages such as the possible mineralisation of a wide range of recalcitrant organics, environmental friendliness, low operational cost and the use of few or no chemicals [25]. The high removal efficiency of organics in PEC degradation is due to the synergistic effect of coupling electrical and light energy [26,27].

The mechanism of production of hydroxyl radicals in PEC is similar to that of heterogeneous photocatalysis. First, semiconducting metal oxides which serve as an anode in PEC are first irradiated with light with greater energy which prompts the excitation of electrons to the conduction band leaving behind holes in the valence band (Equation (1)). Hydroxyl radicals are then produced from the reaction of water molecules present in the reaction medium with the photogenerated holes (Equation (2)). It is obvious then that the production of hydroxyl radicals depends on the amount of photogenerated holes produced from the photoanode. Herein lies the major setback of heterogeneous photocatalysis, in that the availability of photogenerated holes is greatly reduced due to rapid recombination with electrons. However, the application of appropriate external bias potential in the PEC system greatly reduces the recombination rate of photogenerated charge carriers because the potential serves as a driving force in transporting the photogenerated electrons away from the electrode surface and thereby extending the lifetime of photogenerated holes [28,29]. Consequently, the extended lifetime of photogenerated holes in PEC favours the higher production of hydroxyl radicals which help in oxidising organic molecules in the aqueous solution. In as much as holes and hydroxyl radicals often play a predominant role in PEC degradation, there are other reactive oxygen species which are also formed in the reaction systems which also play roles in the mineralisation of the organics. Such reactive oxygen species include superoxide radicals which are formed from the reaction of oxygen molecules with photogenerated electrons in the solution (Equation (3)). Other weaker reactive species are hydroperoxyl radicals and hydrogen peroxide which could be formed according to Equations (4) and (5), respectively [24,28].



Even though PEC combines the principles of photocatalysis and electrochemical oxidation of organics, it has other advantages over these two processes. For instance, in photocatalysis, for powdered or granular photocatalysts to be reused, they must first be recovered or regenerated from the aqueous solution, and this may involve the use of strong chemicals and also it is time-consuming. This problem is overcome in PEC degradation because photocatalysts are used as solid compact electrodes and can easily be rinsed, dried and reused [22]. Furthermore, unlike electrochemical oxidation which could be highly energy-demanding due to the use of the higher cell potential, PEC degradation is more energy efficient because the low applied potential is often used to facilitate the oxidation of organics [30].

In PEC degradation, several kinds of metal oxide semiconductors which are good photocatalysts are often used as photoanodes. Among such materials, several researchers have worked extensively with anatase titanium oxides ( $\text{TiO}_2$ ) as a suitable photoanode for PEC mineralisation of recalcitrant organics [31,32]. A typical PEC degradation setup with  $\text{TiO}_2$  as a photoanode is depicted in Figure 1 [28]. The excitation of electrons from semiconductors only occurs when they are illuminated with light of greater energy than their band gap energy and as it can be seen from the setup, the excitation of bare  $\text{TiO}_2$  is favoured by UV radiation because of its relatively large band gap energy (3.5 eV) [21]. This is the major drawback in the use of  $\text{TiO}_2$  since the solar spectrum is made up of less than 5% UV radiation and UV lamps are expensive. Moreover, human exposure to UV radiation may result in health issues. To make the PEC degradation process safer and more cost-efficient, efforts are channelled towards the use of solar energy as a source of irradiation. This implies that modifications are often applied to  $\text{TiO}_2$  to make it solar light responsive before use for the PEC degradation of organics. In recent studies, such modifications include doping, morphological control and metal loading. These modified  $\text{TiO}_2$  nanostructures will be fully discussed in the next section.

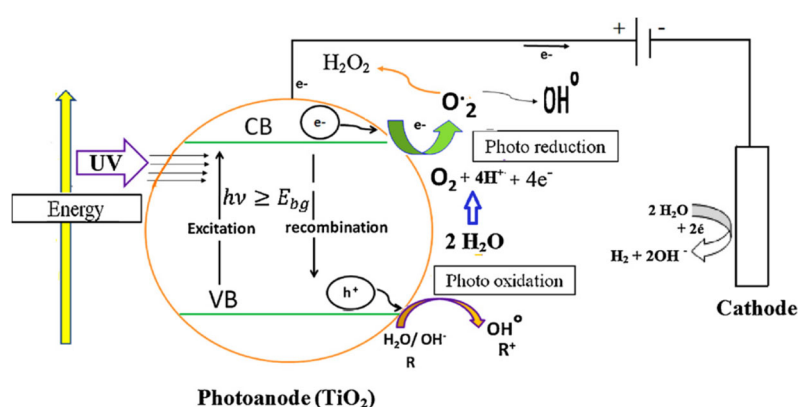


**Figure 1.** General mechanism of photoelectrocatalysis using  $\text{TiO}_2$  as a model photoanode. Reprinted with permission from Ref. [28]. Copyright 2012, Elsevier.

In recent years, much focus has been directed to the application of visible light active metal oxide semiconductors as suitable anodic material for the removal of organic pollutants in an aqueous solution. Since these materials absorb light in the visible light region due to their low band gap, it is possible to harness solar energy as the source of irradiation. This significantly reduces the cost associated with the operation of PEC degradation and it equally makes the process safer since UV irradiation is not needed. Some examples of commonly used visible light responsive metal oxide semiconductors for PEC degradation of organics include  $\text{BiVO}_4$ ,  $\text{WO}_3$ ,  $\text{BiOI}$ ,  $\text{Cu}_2\text{O}$ ,  $\text{MoS}_2$ ,  $\text{Fe}_2\text{O}_3$ ,  $\text{Bi}_2\text{WO}_6$  and  $\text{g-C}_3\text{N}_4$  [33–38]. The application of these visible light active semiconductors will be discussed in this review and the strategies adopted to improve the visible light absorption of the materials towards enhancing their PEC efficiency will also be highlighted.

### 1.2. Essential Characteristics of Photoelectrocatalyst Nanomaterials

Typically, photoanodes in PEC degradation systems often consist of metal oxide semiconductor photocatalysts. However, in a solar light-driven PEC system, the photocatalyst must have a visible light response and this largely depends on the band gap energy of the semiconductor. Ideally, semiconductors with narrow energy band gaps are easily excited with visible light radiation. Additionally, it is expected that the photoanode possesses a higher photo potential than the thermodynamic requirement of water splitting to facilitate the reaction. In some cases, active electrocatalysts are loaded to semiconductors that are catalytically inactive to enable the reaction kinetics and reduce the overpotential for the water-splitting reaction. Hence, essentially, thermodynamics and kinetic issues are critical

factors that must be given serious consideration in the design of a suitable photoanode [39]. Since many visible light-responsive photocatalysts are unstable and could suffer chemical corrosion in the PEC system, the use of protective interlayers to separate the semiconductor and working solutions are common in some PEC systems to enhance the stability of the photoanode. Thus, an ideal photoanode should consist of three layers with distinct functions which include light absorption, surface protection and catalysis. In addition, the photoanode possesses a photoelectrical interface and electrochemical interface. The interface formed between the photoanode and the electrolyte dictates that catalytic processes are the electrochemical interface while the photoelectrical interface is found between the semiconductor and any surface coatings added to promote efficient charge generation and separation.

The properties of nanomaterials used as photoanodes are often assessed through structural, morphological, optical, electrochemical and photoelectrochemical characterisation. Generally, scanning electron microscopy (SEM) and transmission electron microscopy (TEM) coupled with energy dispersive X-ray analysis (EDX) are usually adopted to observe the morphologies of the prepared nanomaterials and their chemical composition. However, it is very vital to confirm if the prepared nanomaterials are capable of visible light absorption and to gain insight into the charge separation mechanism within the materials. This is usually done through UV-visible diffuse reflectance spectroscopy (UV-DRS) and photoluminescence (PL) measurements. It is expected that the nanomaterials absorb photons within the visible light region. Additionally, photocurrent measurements through chronoamperometry are often performed to know the transient photocurrent responses of the material. When a material is modified, a higher photocurrent response is often an indication of improved charge separation which can translate to better PEC efficiencies [22]. In the next sections, the results obtained in the characterisation of the prepared nanostructured photoanodes are discussed.

### 1.3. *TiO<sub>2</sub> Nanostructures in PEC Degradation of Organics*

In as much as TiO<sub>2</sub> photoanodes have been extensively applied for PEC degradation with UV light irradiation, many studies have reported the use of solar light-responsive TiO<sub>2</sub> nanomaterials for PEC degradation of recalcitrant organics. For example, Zhang et al. reported the use of solar light-responsive TiO<sub>2</sub> nanosheets for the PEC degradation of norfloxacin [40]. The TiO<sub>2</sub> nanosheets were prepared through the hydrothermal synthesis in an alkaline environment onto the surface of titanium mesh. The effect of acid washing on the morphology of the prepared nanosheets was also studied by using HCl, HNO<sub>3</sub> and H<sub>3</sub>PO<sub>4</sub> to wash the nanosheets before calcination. The surface morphologies of the samples (Figure 2a–f) revealed that all the samples have a similar lamellate structure suggesting that the acid washing do not affect the morphology and the thickness of the nanosheets which were measured to be within the range of 5 to 20 nm. However, the photocurrent response measurement showed that the TiO<sub>2</sub> nanosheet washed with HNO<sub>3</sub> (TiO<sub>2</sub>-NSs-HNO<sub>3</sub>) has the highest current density of 1.08 mA cm<sup>−2</sup> which indicated that there was a better charge separation in the material (Figure 2g). Upon application of the electrodes, the highest percentage removal of 93% was recorded with a TiO<sub>2</sub>-NSs-HNO<sub>3</sub> photoanode. The initial concentration of norfloxacin was 5 mgL<sup>−1</sup> and a solar light simulator consisting of a 350 W xenon arc lamp was used to irradiate the electrode. It is also interesting to note that the percentage degradation of norfloxacin in the PEC process was significantly higher than what was recorded in photocatalysis (Figure 2h). To gain insight into the improved efficiency in PEC application, a fluorescence technique with terephthalic acid as a probe molecule was used to estimate the amount of hydroxyl radicals produced in the process. The results revealed that a higher amount of hydroxyl radicals was generated in the PEC degradation process than in the photocatalysis which confirmed that nanostructured semiconductors could have a higher degradation efficiency through the PEC process.



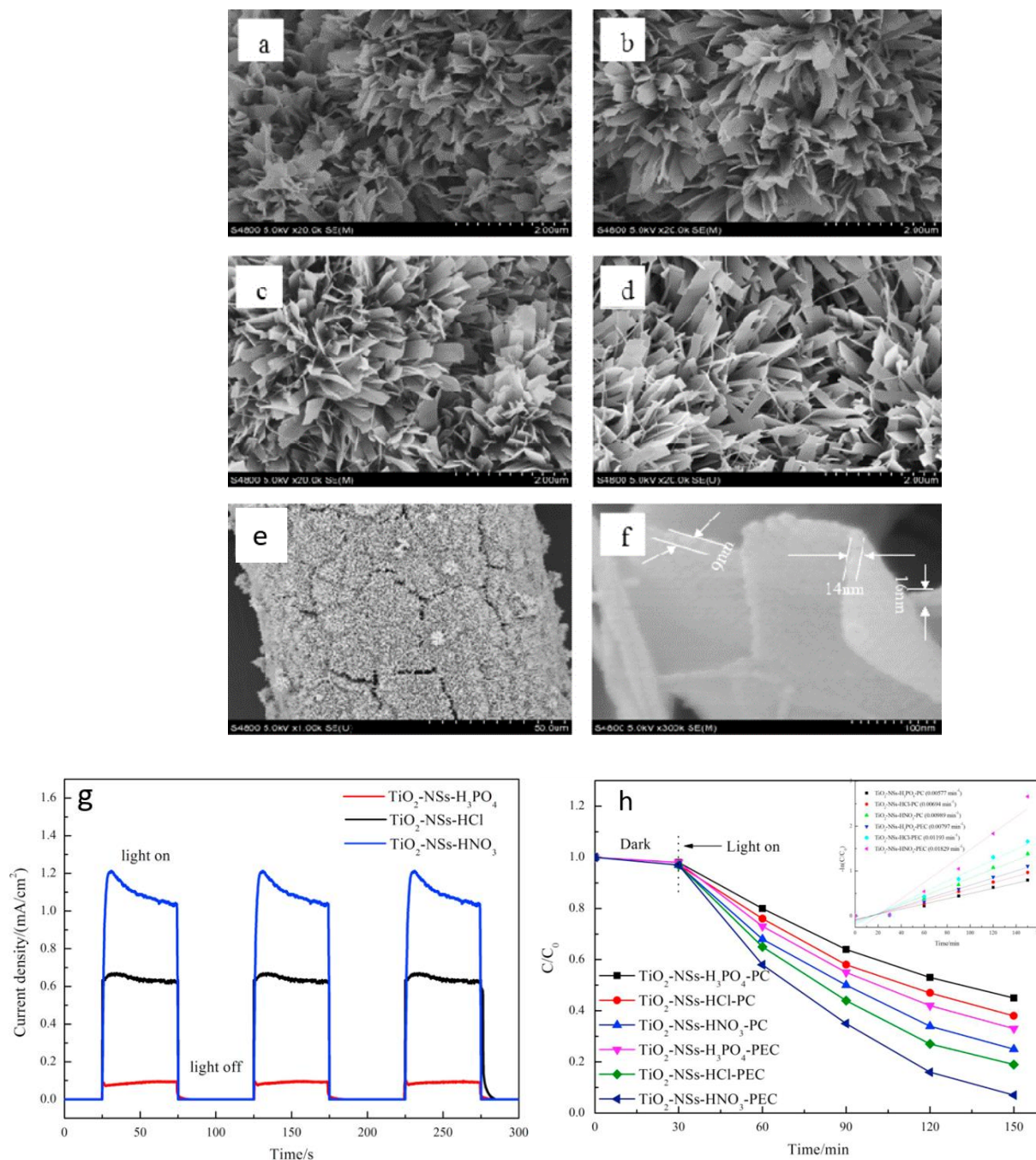


**Figure 2.** SEM images of prepared TiO<sub>2</sub> nanosheets (a) without acid washing, (b) with H<sub>3</sub>PO<sub>4</sub> (c) with HCl, (d) with HNO<sub>3</sub>, (e) low magnification of titanate on Ti mesh, (f) high magnification of TiO<sub>2</sub>-NSs-HNO<sub>3</sub>, (g) photocurrent responses of the photoanodes and (h) concentration decay curve for the removal of norfloxacin. Reprinted with permission from Ref. [40] Copyright 2016, Elsevier.

Several studies involving the use of TiO<sub>2</sub> nanomaterials in PEC degradation under solar light irradiation often involve doping TiO<sub>2</sub> with appropriate metals or non-metals to increase the visible light absorption of TiO<sub>2</sub>. For example, Liu et al. reported the use of iodine-doped TiO<sub>2</sub> (I-TiO<sub>2</sub>) for the PEC degradation of diclofenac using a solar light simulator [41]. The I-TiO<sub>2</sub> was prepared through the hydrolysis method and iodic acid was used as the source of iodine dopant. The morphology of both doped and undoped TiO<sub>2</sub> was similar, having an irregular particle nanostructure. Doping TiO<sub>2</sub> with iodine resulted in the decrease of band gap energy of TiO<sub>2</sub> from 3.18 eV to 2.99 eV which consequently led



to an increase in the visible light absorption of the doped TiO<sub>2</sub>. After a PEC degradation time of 2 h with an applied bias potential of 1.4 V, the I-TiO<sub>2</sub> achieved 99.4% removal of diclofenac with a corresponding TOC removal of 60.2%. These values were approximately six times higher than what was recorded with undoped TiO<sub>2</sub>. In another study, improved PEC degradation efficiency of TiO<sub>2</sub> has also been achieved by doping with iron ions as observed by Xiang et al. [42]. In their work, TiO<sub>2</sub> nanotubes were first prepared by anodization of titanium foil with a constant voltage of 20 V. The prepared TiO<sub>2</sub> nanotubes were subsequently doped with Fe<sup>3+</sup> ions by dip coating in a ferric nitrate solution. The wall thickness of the nanotubes was measured to be 10–15 nm while the internal diameter was around 40–60 nm. The presence of Fe in the nanotubes was confirmed by energy dispersive spectroscopy (EDS). After a PEC degradation time of 4 h, 72.3% removal of bisphenol A was achieved using the Fe-doped TiO<sub>2</sub> while the undoped TiO<sub>2</sub> nanotubes achieved only 58% removal. The higher efficiency of the doped TiO<sub>2</sub> was attributed to better visible light absorption due to its reduced band gap energy which was estimated to be 2.49 eV. Similarly, 98.7% removal of methylene blue within 2 h has been reported with the use of Fe-doped TiO<sub>2</sub> nanotubes under solar light irradiation [43]. In the literature, improved solar light-mediated PEC efficiency of TiO<sub>2</sub> nanomaterials has also been achieved by doping with boron, caesium, nitrogen, sulphur, fluorine and tin [44–48].

Another strategy that is commonly employed to make TiO<sub>2</sub> nanomaterials solar light responsive is loading with plasmonic noble metals such as gold and silver. These noble metals are capable of improving the visible light absorption of TiO<sub>2</sub> through localised surface plasmon resonance. Such metal-loaded TiO<sub>2</sub> nanomaterials have been used as a suitable photoanode for the degradation of organics. For example, Yin et al. applied Au-loaded TiO<sub>2</sub> nanotube arrays (Au/TiO<sub>2</sub>) for the PEC removal of methylene blue [49]. Anodization was first used to obtain the TiO<sub>2</sub> nanotube arrays from a titanium sheet. The microwave-assisted chemical reduction process was then used to deposit Au onto the TiO<sub>2</sub> nanotube arrays from its precursor solution. The wall thickness of the nanotubes was measured to be 44 nm. Upon PEC degradation of methylene blue under simulated solar light irradiation, the Au/TiO<sub>2</sub> anode achieved 66% removal efficiency while the bare TiO<sub>2</sub> electrode removed only 40% of the dye concentration. Au nanoparticles also serve as photosensitizers producing high-energy electrons with solar light illumination and greatly enhancing the PEC efficiency of TiO<sub>2</sub>. In a similar study conducted by Wang et al., composites of Ag-Au (alloys and core-shell) were used to improve the PEC performance of the TiO<sub>2</sub> nanotube array [50]. After obtaining TiO<sub>2</sub> nanotube arrays through anodization, UV light reduction followed by a metal displacement reaction was used to introduce Ag-Au alloys and a core-shell into the TiO<sub>2</sub> nanotubes. Both the TiO<sub>2</sub> with an Ag-Au alloy and TiO<sub>2</sub> with an Ag@Au core-shell performed better than pristine TiO<sub>2</sub> nanotube arrays achieving a PEC removal of 89.7% and 98.1% of methyl orange, respectively. These results further affirm that loading TiO<sub>2</sub> with plasmonic noble metals significantly increases its visible light activity. It is worth noting that other metals, non-metals and semiconductors can also be loaded onto the TiO<sub>2</sub> nanostructure to improve its performance. For example, silicon, a semiconductor, has been used to improve the PEC efficiency of the TiO<sub>2</sub> nanostructure as reported by Chen et al. [51]. The Si/TiO<sub>2</sub> photoanode was prepared using a hydrothermal route. The prepared photoanode was successfully used to degrade methylene blue under solar light illumination.

Additionally, suitable conductive polymers have been effectively used to increase the visible light absorption of TiO<sub>2</sub> nanomaterials. A typical example of a commonly used conductive polymer is polyaniline (PANI). Wang et al., reported the PEC degradation of phenol with simulated light irradiation using PANI/TiO<sub>2</sub> as an electrode [52]. The PANI nanosheet-wrapped TiO<sub>2</sub> nanotube arrays were prepared through electrochemical anodic oxidation and vacuum-assisted impregnation. The SEM images revealed that TiO<sub>2</sub> nanotubes were uniformly wrapped with PANI nanosheets forming a core-shell structure. The PANI/TiO<sub>2</sub> photoanode achieved 83% PEC removal of phenol after 3 h with simulated solar light illumination and a bias potential of 1.0 V. This percentage removal

was significantly higher than what was observed with the use of a TiO<sub>2</sub> nanotube. The results confirm that PANI increases the PEC efficiency of TiO<sub>2</sub> through better harvesting of visible light. Another conducting polymer that has been used to improve the PEC efficiency of TiO<sub>2</sub> under solar light irradiation is polypyrrole as reported by Zhang et al. [53]. After the anodization of the titanium plate to obtain TiO<sub>2</sub> nanotube arrays, polypyrrole was electropolymerized on the surface of the TiO<sub>2</sub> nanotubes. The composite electrode achieved 100% decolourisation of methylene blue within 60 min through PEC degradation. The impressive PEC efficiency of the anode was attributed to better light harvesting and enhanced charge separation due to the presence of polypyrrole. Recently, Sboui et al. reported the application of PANI/TiO<sub>2</sub> for the degradation of methylene blue and methyl orange through the photoelectrocatalysis process coupled with membrane filtration under solar light illumination [54]. It was observed that the composite photoanode possessed impressive photoelectrochemical properties and the percentage degradation of the two dyes recorded within 1 h was over 70%. These results showed that nanostructured TiO<sub>2</sub> composites with appropriate modifications are still ideal as photoanodes in solar light-mediated photoelectrocatalysis.

#### 1.4. Zinc Oxides Nanomaterials as Photoanodes

Zinc oxide is another common semiconductor photocatalyst that has been widely used for water treatment applications. The interest in ZnO can rightly be justified given its impressive properties such as good thermal stability, large surface area and good electron mobility. In addition to these, ZnO is non-toxic, abundant in nature and easy to synthesize. However, as with TiO<sub>2</sub>, the use of ZnO nanomaterials in PEC water treatment applications is impeded by its relatively large band gap energy of 3.37 eV. Therefore, most PEC degradation of organics use ZnO anodes and applied UV illumination for better degradation efficiency. For instance, ZnO photoanodes have been successfully used to degrade p-nitrophenol [55], methylene blue [56] and terephthalic acid [57] in aqueous solutions with UV irradiation. To facilitate PEC degradation using ZnO photoanodes with solar light, appropriate strategies are often employed to improve the visible light photocatalytic activity of ZnO.

A suitable strategy for improving visible light absorption of ZnO towards PEC application is doping with appropriate metals or non-metals. Nickel has been successfully used to dope ZnO for PEC degradation of organics as reported by Feng et al. [58]. The Ni-doped ZnO was prepared through liquid phase deposition onto FTO glass and calcination at 500 °C. The prepared Ni-ZnO consisted of prismatic nanoparticles as confirmed with the microscopic imaging technique and displayed stronger absorption in the visible light region within the range of 400 nm to 525 nm. The prepared doped material showed enhanced photoelectrochemical properties with visible light illumination as indicated in pronounced photocurrent responses recorded at a potential range of 0.2 V to 1.2 V, which confirmed that nickel improved visible light absorption. The Ni-ZnO electrode was then applied to degrade tetracycline through PEC with an applied bias potential of 0.8 V under visible light illumination. After a PEC treatment time of 3 h, 87.5% removal of tetracycline was recorded, and this value was 17% higher than PEC treatment with undoped ZnO. These results confirmed that ZnO nanomaterials when doped with Ni could find practical applications for PEC degradation of a recalcitrant organic in an aqueous medium with the use of solar light illumination. It is interesting to note that a similar enhanced performance of Ni-doped ZnO has been reported with the use of ciprofloxacin as a target analyte [59]. In another study conducted by Gholami et al. [60] where the PEC degradation efficiency of Ni-doped ZnO was compared under both UV irradiation and visible light radiation, it was evident that Ni-doped ZnO performed better with UV irradiation. Specifically, 98% and 64% degradation efficiencies were achieved under UV and visible light radiation, respectively. In addition, palladium-modified ZnO prepared through atomic layer deposition (ALD) has been employed in the PEC degradation paracetamol under solar light irradiation [61]. The addition of Pd significantly improved the visible light responsiveness of ZnO as clearly observed through UV/Vis- diffuse reflectance spectrophotometry. Consequently, the modi-

fied ZnO photoanode achieved complete removal of paracetamol within 3 h and the extent of mineralization was found to be 71% through the measurement of total organic carbon.

Plasmonic noble metals have also been used to improve the PEC efficiency of ZnO nanomaterials under visible light illumination. For example, Trang et al. reported the PEC degradation of rhodamine B dye under visible illumination using Ag-modified ZnO [62]. Ag nanoparticles were anchored onto ZnO nanosheets using the radio frequency sputtering method without subsequent thermal treatment. From the morphological study, the particle size of the composite material was measured to be within the range of 50 to 100 nm. The nanostructured Ag@ZnO showed good photon absorption within 400 to 500 nm, as observed in its diffuse reflectance spectrum, indicating that the prepared material would be suitable for application using solar light or other visible light exposure. This was further demonstrated using the Ag@ZnO electrode to degrade rhodamine B with an initial concentration of  $20 \text{ mgL}^{-1}$  under visible light exposure. After a reaction time of 2 h, 82% removal of rhodamine B was recorded using the composite material and the recorded efficiency was significantly higher than that achieved with pristine ZnO. The improved performance of Ag@ZnO was attributed to the Ag nanoparticles which created a localized surface plasmon resonance and equally served as an electron sink which led to the effective separation of a photogenerated charge carrier. Additionally, cobalt (another transition metal) has also been used to enhance the visible light absorption of ZnO as reported by Tian et al. where 86.7% PEC removal of ofloxacin was achieved with visible light irradiation after a reaction time of 6 h [63]. Certainly, ZnO has great prospects for PEC degradation of organics with solar light illumination.

### 1.5. Tungsten Trioxides Nanostructured Photoanodes

In recent years, significant attention has been given to ways of utilising solar energy as a source of illumination in PEC water treatment applications and this has led to concerted efforts in the use of visible light active semiconductor photocatalysts as anodic material. An example of such is tungsten trioxide ( $\text{WO}_3$ ).  $\text{WO}_3$  has been identified as a suitable photoanode for harnessing solar energy due to its low band gap energy which lies between 2.5 to 2.8 eV. Additionally, it has other impressive properties such as good chemical and photochemical stability even in an acidic environment [64]. Photoanodes of nanostructured  $\text{WO}_3$  have been successfully applied for the PEC degradation of a vast range of organic pollutants under simulated solar light irradiation. As an example, Zeng et al. have studied the PEC degradation of methylene blue using  $\text{WO}_3$  nanoplate array films [65]. The  $\text{WO}_3$  films were prepared onto FTO glass using a hydrothermal route which was followed by annealing at different temperatures. The prepared photoanode was used to degrade methylene blue at a bias potential of 1 V under visible light irradiation from a solar simulator. The percentage of PEC removal was almost 80% in less than 2 h.

Another dye that has been successfully degraded using the  $\text{WO}_3$  photoanode is brilliant blue as reported by Hunge et al., where 92% PEC degradation of the dye was achieved within 4 h with visible light illumination [66]. The nanostructured  $\text{WO}_3$  electrode was prepared by spray pyrolysis onto FTO glass. It was also observed that improved PEC efficiency was dependent on the thickness of the  $\text{WO}_3$  and this was equally confirmed by the increase in the band gap energy with an increase in the film thickness. In another similar study, the PEC degradation of methyl blue using a photoanode consisting of  $\text{WO}_3$  thin films was carried out [67]. The photoanode was prepared through spray pyrolysis by spraying a precursor solution of  $\text{WO}_3$  onto preheated FTO glass. The average crystallite size of the prepared  $\text{WO}_3$  was 27 nm and displayed good absorption of photons in the visible light region; therefore, the photoanode was applied to degrade methyl blue with visible light illumination. After 2 h, the percentage removal of the dye was 98.56%, which confirmed the efficiency of PEC and the kinetics study revealed that the degradation process using the electrode is fast and spontaneous. The impressive mineralisation of rhodamine B using  $\text{WO}_3$  has also been reported [68]. In addition,  $\text{WO}_3$  photoanodes have been efficient in the removal of organic dyes.

Photoanodes of WO<sub>3</sub> nanostructures have also been successfully applied for the PEC removal of several kinds of pesticides. For example, the photoanode of WO<sub>3</sub> nanostructures have been successfully used for the degradation of diuron, a persistent herbicide, as reported by Fernandez-Domene et al. [69]. The WO<sub>3</sub> photoanode was prepared through anodization of a tungsten rod at 20 V for 4 h using a hydrogen peroxide solution. The obtained WO<sub>3</sub> consisted of several nanoplatelets with length and width dimensions of  $626 \pm 25$  nm and  $29.2 \pm 1.2$  nm, respectively. The PEC degradation of 20 mgL<sup>-1</sup> of diuron solution was performed with a bias potential of 1 V under simulated solar light. After a reaction time of 6 h, the percentage removal of diuron was about 73% using the prepared WO<sub>3</sub> photoanode. The extent of mineralisation of diuron was estimated to be approximately 50% using ionic chromatography. Similarly, photoanodes consisting of WO<sub>3</sub> nanorods have been used to degrade fenamiphos, chlorfenvinphos and phosmet pesticides [70,71]. The WO<sub>3</sub> photoanode was also prepared through an anodization technique with a hydrogen peroxide solution. The results obtained from PEC degradation with visible light illumination were very impressive as they revealed that the WO<sub>3</sub> nanostructured anode achieved 100% removal of the pesticide within 2 h. The degradation processes were found to follow the pseudo-first-order kinetics and analyses of the degradation products and confirmed that the pesticides were broken down into non-toxic organic compounds. The same research group subsequently confirmed the possibility of using a WO<sub>3</sub> photoanode to degrade a mixture of pesticides in an aqueous solution [72]. Hence, WO<sub>3</sub> nanostructures have great potential in degrading persistent organic pollutants.

To further improve the PEC efficiency of WO<sub>3</sub> nanostructured anodes with visible light illumination, appropriate materials have been used as dopants. Gallium (Ga), for example, has been used to dope WO<sub>3</sub> to improve PEC performance as reported by Mohite et al. [73]. The Ga-doped WO<sub>3</sub> was prepared by spray pyrolysis on FTO glass. The Ga-doped WO<sub>3</sub> has an average particle size of 67 nm and displayed a better photocurrent response than the undoped WO<sub>3</sub> which revealed that there was a better separation of photogenerated electron-hole pairs in the Ga-doped WO<sub>3</sub>. The incorporation of Ga into WO<sub>3</sub> led to better absorption of light within the visible light region which was confirmed by the shift of absorption edge to a higher wavelength in the UV diffuse reflectance spectrum. Consequently, higher mineralisation of benzoic acid and salicylic acid was achieved with the use of Ga-doped WO<sub>3</sub> in PEC degradation than the undoped WO<sub>3</sub>. In another study, nitrogen has been used as a dopant for nanoporous WO<sub>3</sub> [74]. The rate of degradation of methyl orange using the N-doped WO<sub>3</sub> was found to almost double that of undoped WO<sub>3</sub>. Therefore, it can be inferred that doped WO<sub>3</sub> nanostructures are excellent anodes for the PEC degradation of organics.

In another study, the improved PEC degradation efficiency of WO<sub>3</sub> nanostructured electrodes was achieved through the use of exfoliated graphite as the conducting substrate [75]. The WO<sub>3</sub> nanoparticles were first synthesised using a simple chemical precipitation technique. The prepared WO<sub>3</sub> was then combined with exfoliated graphite to form a composite with the aid of sonication. The structural and morphological examination revealed that irregular rhombic structured monoclinic WO<sub>3</sub> nanoparticles were formed with an average crystallite size of 24.7 nm. In the composite material, the nanoparticles of WO<sub>3</sub> were well observed to be evenly dispersed within the interlayers of the graphite sheets. The composite material showed better visible light harvesting properties than the pristine WO<sub>3</sub> and this gave evidence of improved photoactivity. This was further confirmed through the photocurrent response measurement under simulated solar light and the composite electrode gave a higher photocurrent of about 0.5 mA cm<sup>-2</sup>. This improved photocatalytic property was attributed to the fact that the exfoliated graphite facilitated better light harvesting in the WO<sub>3</sub> by enhancing effective electron transfer which consequently limited the spontaneous recombination of photogenerated charge carriers. Upon application of the composite electrode in the PEC degradation of organics, the percentage removal of orange II dye and 2-nitrophenol were 95% and 82% after 3 h under simulated solar light illumination. The recorded PEC efficiency obtained with the composite electrode



revealed that exfoliated graphite is a suitable material for enhancing the photocatalytic activity of  $\text{WO}_3$ .

#### 1.6. Bismuth Vanadate Nanostructures as Photoanodes

Bismuth vanadate ( $\text{BiVO}_4$ ) is another common visible light active semiconductor that has found remarkable applications in the field of photoelectrochemical studies. Pronounced interest in the use of  $\text{BiVO}_4$  can be attributed to its good photocatalytic, optical and ionic conductivity properties. Monoclinic  $\text{BiVO}_4$  has a small band gap energy of around 2.4 eV which facilitates good absorption of visible light. Additionally,  $\text{BiVO}_4$  has an appropriate position valence band which makes it a choice material for hydrogen evolution in water-splitting applications [76]. Photoanodes of the  $\text{BiVO}_4$  nanostructure have been successfully used for PEC degradation of phenols, dyes and pharmaceuticals in wastewater. As an example, Deshpande et al. reported the use of the  $\text{BiVO}_4$  photoanode for the removal of azo dyes under visible light illumination [77]. The nanostructured  $\text{BiVO}_4$  anode was prepared by spinning and coating FTO glass with a precursor solution containing a mixture of bismuth salt and vanadate solution. The spin-coated FTO glass was then annealed at 500 °C. The ratio of bismuth and vanadium in the samples was also varied to obtain different nanostructures of  $\text{BiVO}_4$ . Interestingly, the  $\text{BiVO}_4$  sample containing Bi and V in the ratio of 1 to 3 shows the highest absorbance in the visible light region and it has nanoporous dual morphology of multi-faceted nanospheres and a sheet-like decahedral. The prepared photoanode was used to degrade 20 mg  $\text{L}^{-1}$  each of Congo red and methylene blue under simulated sunlight. After 6 h, the percentage of PEC removal was 96% for methylene blue while 86% of Congo red was removed in 90 min. The impressive PEC efficiency recorded was attributed to the larger surface area which was achieved by controlling the morphology of the nanostructured  $\text{BiVO}_4$ .

In another study reported by Xia et al., a nanostructured  $\text{BiVO}_4$  photoanode was used to mineralise dyes and for the simultaneous generation of electricity [78]. The  $\text{BiVO}_4$  anode was prepared through a two-step electrodeposition technique which was followed by annealing at 450 °C. The thickness of the nanoporous film was found to be less than 1  $\mu\text{m}$  with an average pore size of 70 nm. For the PEC degradation experiment, the prepared  $\text{BiVO}_4$  was used as a photoanode while the gold-decorated photovoltaic cell (Au/PVC) served as the photocathode under simulated solar light illumination. Impressively, after a reaction time of 2 h, the percentage of PEC removal for methylene blue, methyl orange and rhodamine B dye was 93.2%, 89.15% and 77.98%, respectively. These PEC removal values were significantly greater than what was achieved using a platinum sheet as cathode and this implied that the PEC efficiency of  $\text{BiVO}_4$  can be further enhanced using different strategies in the PEC setup. However, in the works of Bacha et al, the PEC efficiency using the  $\text{BiVO}_4$  photoanode was simply enhanced by the addition of sulphite [79]. In the presence of 16 mM sulphite, 96.6% removal of methyl orange was recorded after 2 h compared to the 10.9% removal observed in the absence of sulphite.

It has been further observed that the PEC efficiency of  $\text{BiVO}_4$  nanostructures is greatly affected by the rapid recombination of photogenerated electron-hole pairs as well as its poor adsorptive property. Coating  $\text{BiVO}_4$  with metals, which serves as a protective layer, has been identified as a way of improving its performance. For instance, Bacha et al. compared the PEC efficiency of pristine  $\text{BiVO}_4$ , in which  $\text{BiVO}_4$  is coated with cobalt, nickel and iron [80]. The nanostructured  $\text{BiVO}_4$  was first prepared by dip-coating using a precursor solution followed by annealing. The metal-coated  $\text{BiVO}_4$  was prepared through the impregnation method. The microscopic image of the prepared materials revealed that all the materials have irregularly shaped particles. However, in the metal-loaded  $\text{BiVO}_4$ , small particles of metals were observed which confirmed the successful coating of  $\text{BiVO}_4$  (Figure 3a). The prepared photoanodes were used to degrade 20 mg  $\text{L}^{-1}$  of bisphenol A under simulated solar light irradiation in the presence of peroxydisulfate. After 60 min, the percentage of PEC removal of BPA was found to be 99.16% using the Co- $\text{BiVO}_4$ . Though the highest PEC efficiency was observed with Co- $\text{BiVO}_4$  due to the standard reduction

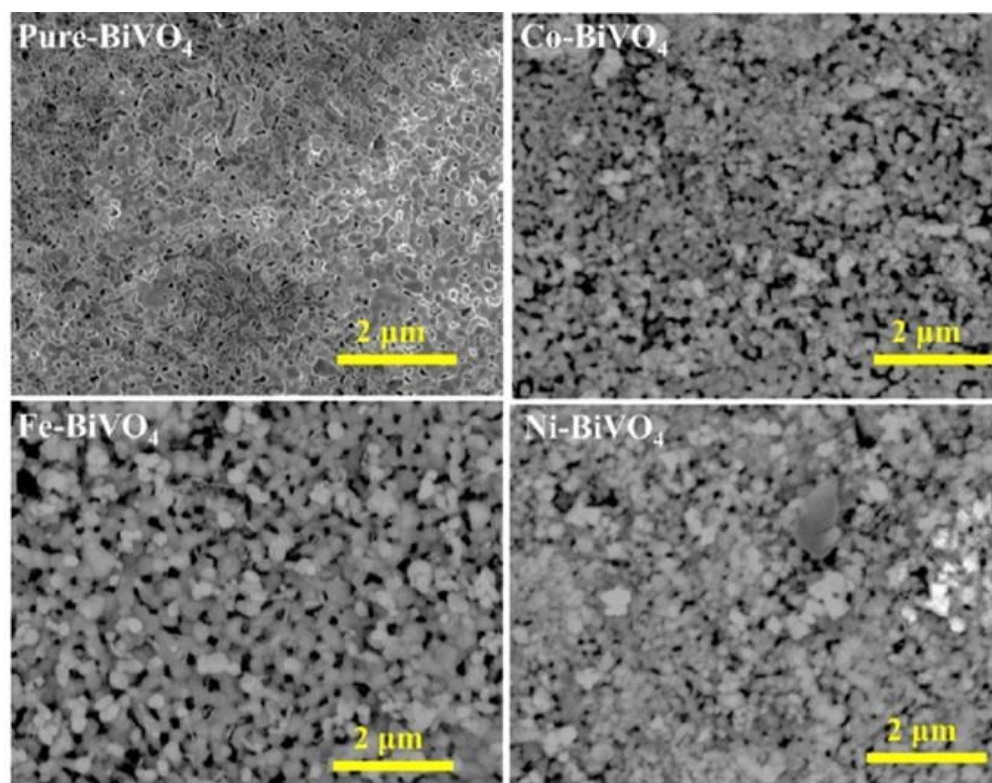


potential of Co ions, all the metal-coated  $\text{BiVO}_4$  anodes performed better than the pure  $\text{BiVO}_4$  (Figure 3b). Furthermore, the degradation intermediate products were determined to confirm the degradation of bisphenol A and proposed the degradation pathways. It was observed that non-toxic lower-chain hydrocarbons were produced through hydroxylation, C-C bond breakage, dihydroxylation and aromatic ring breakage. These results confirmed that coating  $\text{BiVO}_4$  nanostructures with transition metals could enhance their PEC performance for the degradation of organics.

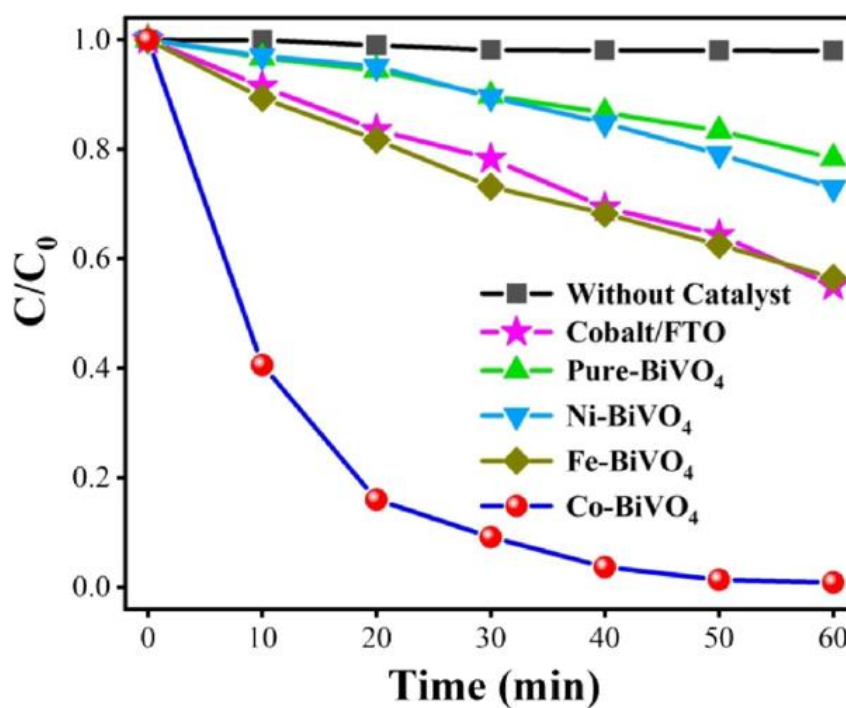
### 1.7. Nanostructured Semiconductors Heterojunctions

The use of visible light active semiconductor photocatalysts has significantly made possible the use of solar light illumination in PEC water treatment applications. However, the efficiency often recorded with unmodified visible light-responsive photocatalysts is still below expectations. This is because these semiconductors suffer significantly from the problem of instantaneous recombination of photogenerated electron-hole pairs. Among several strategies that have been used to circumvent this problem, the fabrication of a semiconductor–semiconductor heterojunction has attracted wide interest due to its advantages and impressive results obtained from its use [81]. A semiconductor–semiconductor heterojunction is formed when two semiconductors of unequal band gap energy are combined in such a way that results in band alignment [82]. Due to this band alignment, holes and electrons can be effectively separated into different semiconductors. The common band alignment is often applied in photocatalysis and PEC are either Type II or Z-scheme which often result in good efficiency [83,84]. However, the semiconductor–semiconductor heterojunction can also be classified as a p-p, p-n or n-n heterojunction depending on the types of semiconductors combined. As summarized by Arotiba et al., heterojunctions have been used extensively in PEC water treatment in the recent year [85].

Semiconductor heterojunctions have been extensively used for the PEC degradation of several kinds of organic dyes. As an example, the PEC degradation of methyl orange dye under visible light irradiation using an n-n heterostructured photoanode of  $\text{MnO}_2/\text{TiO}_2$  nanotube arrays has been reported. The  $\text{MnO}_2/\text{TiO}_2$  was prepared by first performing the anodization of a titanium plate to obtain  $\text{TiO}_2$  nanotube arrays and  $\text{MnO}_2$  was then electrodeposited onto the  $\text{TiO}_2$  nanotube arrays. The morphological study revealed that the prepared  $\text{TiO}_2$  nanotube arrays had an average wall thickness of 60 nm and an inner diameter of 300 nm while the  $\text{MnO}_2$  nanoparticles of an average size of 8 nm were uniformly dispersed on the surface of the  $\text{TiO}_2$  nanotube arrays. To assess the extent of charge separation and rapid recombination of photogenerated electron-hole pairs, the transient photocurrent responses of the bare  $\text{TiO}_2$  and  $\text{MnO}_2/\text{TiO}_2$  heterostructured anodes were recorded using simulated solar light. The photocurrent densities of  $\text{TiO}_2$  and  $\text{MnO}_2/\text{TiO}_2$  electrodes were  $0.41 \text{ mA cm}^{-2}$  and  $0.52 \text{ mA cm}^{-2}$ , respectively. The obvious larger photocurrent density of the  $\text{MnO}_2/\text{TiO}_2$  electrode revealed that the formation of a heterojunction between  $\text{MnO}_2$  and  $\text{TiO}_2$  promoted the improved separation of the photogenerated charge carriers. The improved charge separation further led to better PEC degradation efficiency when the electrode was used to degrade methylene blue. The percentage removal of the dye was 95.2% after 60 min using  $\text{MnO}_2/\text{TiO}_2$  while a lesser percentage of 77.8% was recorded with bare  $\text{TiO}_2$  nanotube arrays. The mechanism of the charge separation in the heterojunction confirmed that a type I band alignment was formed where the electrons in the conduction band of  $\text{TiO}_2$  migrated to the conduction band of  $\text{MnO}_2$  and thereby make available more holes to facilitate PEC degradation.



(a)



(b)

**Figure 3.** (a) SEM images of BiVO<sub>4</sub> and BiVO<sub>4</sub> loaded with Ni, Co and Fe. (b) Corresponding concentration decay curve for the PEC removal of bisphenol A using the metal loaded BiVO<sub>4</sub> anodes. Reprinted with permission from Ref. [80]. Copyright 2020, Elsevier.

In another study, the PEC degradation of methylene blue dye was investigated under visible light irradiation, and  $\text{Ag}_3\text{PO}_4/\text{Ag}_4\text{P}_2\text{O}_7$  nanospheres deposited on  $\text{TiO}_2$  nanotube arrays were used as the photoanode [86]. The heterostructured photoanode was prepared by deposition of  $\text{Ag}_3\text{PO}_4/\text{Ag}_4\text{P}_2\text{O}_7$  nanoparticles on the surface of  $\text{TiO}_2$  nanotube arrays through the hydrothermal method and cetyltrimethylammonium bromide (CTAB) was used as a surfactant to control the morphology and size of the  $\text{Ag}_3\text{PO}_4/\text{Ag}_4\text{P}_2\text{O}_7$  nanospheres. The  $\text{TiO}_2$  nanotube arrays have an average diameter of 100 nm and a wall thickness of 8 nm while the average size of the  $\text{Ag}_3\text{PO}_4/\text{Ag}_4\text{P}_2\text{O}_7$  nanosphere was 35 nm. The composite anode displayed a high solar absorption intensity and enhanced PEC performance which was seen in a higher photocurrent density of  $101.51 \mu\text{A cm}^{-2}$  recorded with simulated solar light illumination. The enhanced PEC performance resulted in 99.39% decomposition of methylene blue within 40 min with a low applied bias potential of 0.5 V and photogenerated holes and superoxide radicals played significant roles in the degradation of the dye. This impressive PEC degradation efficiency was attributed to the reduction of rapid recombination of photogenerated electron-hole pairs as a result of the formation of a type II heterojunction between  $\text{TiO}_2$  nanotube arrays and  $\text{Ag}_3\text{PO}_4/\text{Ag}_4\text{P}_2\text{O}_7$  nanospheres.

Fei et al. also reported the PEC degradation of acid red 1 dye using an anode consisting of  $\text{ZnO}/\text{MoS}_2$  with a p-n heterojunction [87]. The photoanode was prepared by facile immobilization of  $\text{ZnO}$  nanosheets and  $\text{MoS}_2$  nanoparticles on nickel foam through a two-step electrodeposition as depicted in Figure 4a. The morphology of the electrode confirmed the uniformity of  $\text{ZnO}$  nanosheets on the Ni foam as well as the presence of well-distributed  $\text{MoS}_2$  nanoparticles. The results from the optical analysis revealed that the  $\text{ZnO}/\text{MoS}_2$  electrode absorbed photons more in the visible light region, unlike the  $\text{ZnO}$  electrode which gave evidence of a charge separation due to an increase in interfacial charge transfer within the p-n junction. This was further confirmed with the photocurrent response measurement under visible light illumination. The heterostructured photoanode gave an impressive photocurrent density which was approximately eight times higher than what was recorded with the  $\text{ZnO}$  photoanode. The efficient charge separation which led to enhanced PEC performance equally resulted in 100% PEC removal of  $20 \text{ mg L}^{-1}$  acid red 1 dye within 40 min. The effective charge separation within the interface of  $\text{MoS}_2$  and  $\text{ZnO}$  in the heterojunction can be seen in Figure 4b with the corresponding percentage PEC degradation of rhodamine B shown in 4c. In another study, rhodamine B dye was also successfully degraded using nanostructured  $\text{BiVO}_4/\text{ZnO}$  [88] and  $\text{BiVO}_4/\text{Cu}_2\text{O}$  [89] heterojunctions. Evidently, significant successes have been recorded in the use of nanostructured heterojunction anodes in the PEC degradation of dyes.

Heterostructured photoanodes have also been applied for PEC degradation on a wide range of pharmaceuticals under visible light illumination. For example, penicillin G, an antibiotic, has been successfully degraded using a photoanode of  $\text{CuS}/\text{TiO}_2$  nanotube arrays consisting of a p-n heterojunction [90]. The  $\text{TiO}_2$  nanotube arrays were first prepared by anodization of titanium plate and  $\text{CuS}$  nanoparticles were subsequently electrodeposited on the  $\text{TiO}_2$  nanotube arrays to obtain the heterostructured anode. The formation of a p-n heterojunction led to an increase in the specific surface area from  $8.9 \text{ cm}^2 \text{ g}^{-1}$  to  $13.5 \text{ cm}^2 \text{ g}^{-1}$  which could enhance the PEC process. Improved PEC efficiency was seen in the transient photocurrent response measurement. The recorded photocurrent densities were  $0.067 \text{ mA cm}^{-2}$  and  $0.097 \text{ mA cm}^{-2}$  for  $\text{TiO}_2$  and  $\text{CuS}/\text{TiO}_2$  electrodes, respectively. The higher values obtained with  $\text{CuS}/\text{TiO}_2$  suggest an increase in the concentration of photogenerated charge carriers due to improving the separation of charge carriers within the heterojunction interface. This was supported by the charge carrier densities estimated from Mott Schottky's measurement where the values were  $0.74 \times 10^{19} \text{ cm}^{-3}$  and  $1.44 \times 10^{19} \text{ cm}^{-3}$  for  $\text{TiO}_2$  and  $\text{CuS}/\text{TiO}_2$  electrodes, respectively. As a result of the better charge separation due to the formation of p-n heterojunction in the  $\text{CuS}/\text{TiO}_2$  electrode, upon PEC degradation of penicillin G, 99.1% removal was achieved within 4 h.

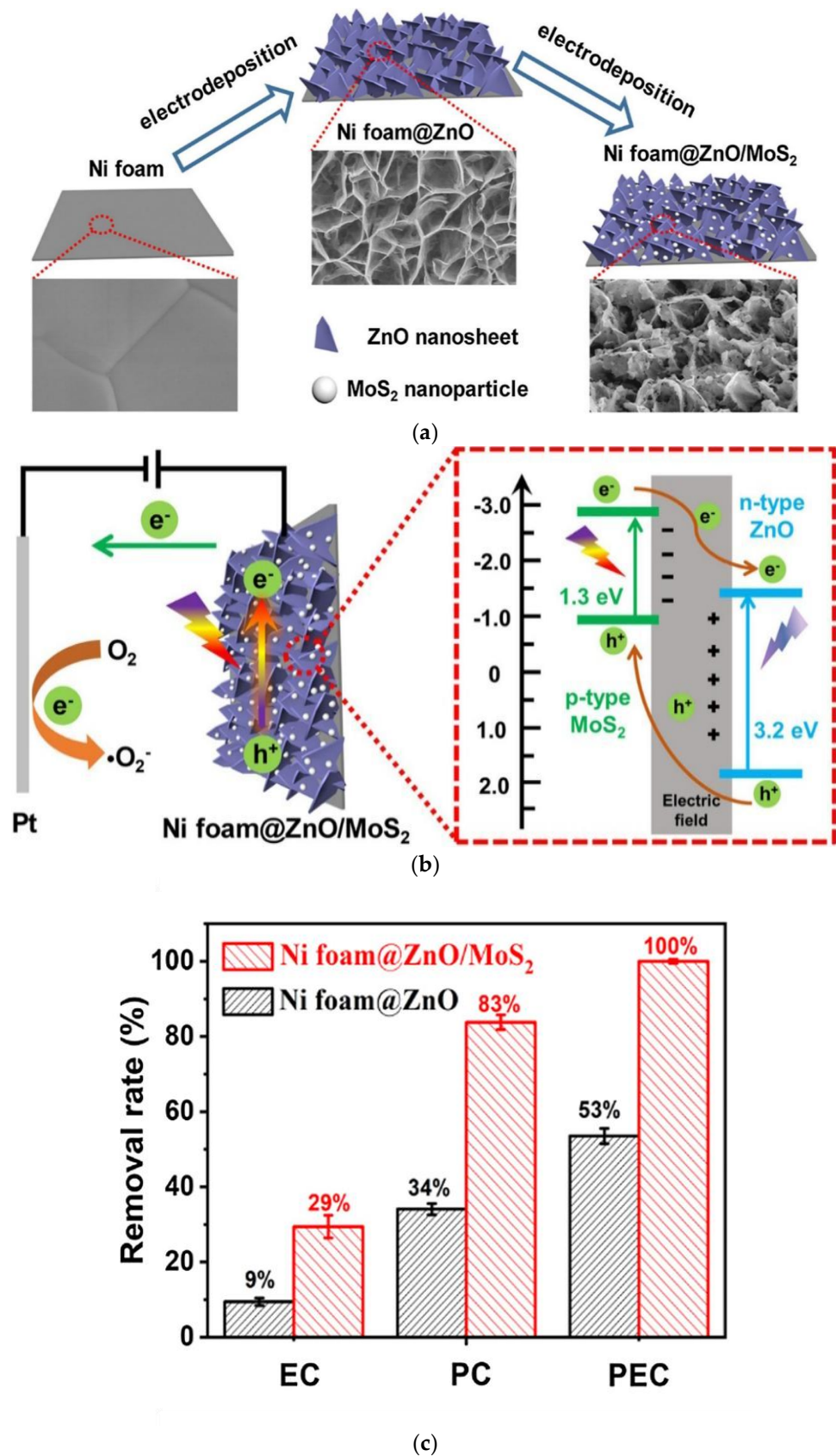


**Figure 4.** (a) Schematic preparation of the MoS<sub>2</sub>/ZnO heterojunction on nickel foam; (b) mechanism of charge separation within the MoS<sub>2</sub>/ZnO heterojunction and (c) percentage PEC removal of rhodamine B using ZnO and MoS<sub>2</sub>/ZnO prepared on Ni foam. Reprinted/adapted with permission from Ref. [87]. Copyright 2020, Elsevier.



In another study conducted by Adhikari et al., the PEC degradation of tetracycline was achieved using a solar-responsive photoanode consisting of a  $\text{Fe}_2\text{O}_3/\text{Bi}_2\text{WO}_6$  heterojunction. The  $\text{Bi}_2\text{WO}_6$  nanoflakes were first prepared through the hydrothermal method and spin-coated on FTO glass to obtain an electrode [91]. The atomic layer deposition of  $\text{Fe}_2\text{O}_3$  was then performed on the FTO glass with  $\text{Bi}_2\text{WO}_6$  to obtain the  $\text{Fe}_2\text{O}_3/\text{Bi}_2\text{WO}_6$  heterojunction. The morphological studies of the material revealed that  $\text{Bi}_2\text{WO}_6$  were nanoflakes with an average thickness of approximately 28 nm and were uniformly coated with  $\text{Fe}_2\text{O}_3$  particles. From the optical studies, the band gap energy of  $\text{Bi}_2\text{WO}_6$  was reduced from 2.76 eV to 2.28 eV in the heterojunction which resulted in better visible light absorption. The  $\text{Fe}_2\text{O}_3/\text{Bi}_2\text{WO}_6$  equally gave a better transient photocurrent response than pristine  $\text{Bi}_2\text{WO}_6$  due to better charge separation which reduced a recombination of an photoexcited electron–hole pair. The percentage of PEC degradation of tetracycline using the heterostructured photoanode was 95% while the bare  $\text{Bi}_2\text{WO}_6$  was 59% within 90 min. The improved PEC efficiency was attributed to the formation of a p-n heterojunction which led to the efficient separation of photogenerated charge carriers. Similarly, 90% PEC removal of tetracycline under visible light radiation within 90 min [92] and 85% removal within 60 min [93] using  $\text{BiVO}_4/\text{ZnO}$  heterostructured photoanodes has been observed. Likewise, a  $\text{BiOI}/\text{MnO}_2$  photoanode with a p-n heterojunction has been used to achieve 94% removal of tetracycline within 2 h [94]. It was noted that the formation of the heterojunction was responsible for the remarkable performance. Importantly, the extent of mineralization of the pharmaceutical was found to be 61% according to the total organic carbon removal.

Another common antibiotic that has been successfully degraded using the PEC process with heterostructured photoanode is ciprofloxacin. For example,  $\text{BiVO}_4/\text{MnO}_2$  with an n-n heterojunction has been used to degrade ciprofloxacin as reported by Orimolade et al. [95]. The nanostructured photoanode with a n-n heterojunction was prepared through a two-step electrodeposition. First,  $\text{BiVO}_4$  was deposited on FTO glass which was followed by the deposition of  $\text{MnO}_2$ . The structural and morphological study revealed that nanoparticles of monoclinic scheelite  $\text{BiVO}_4$  were entrapped within the cracks of birnessite  $\text{MnO}_2$ . Clear evidence of improved visible light harvesting in the  $\text{BiVO}_4/\text{MnO}_2$  was seen in the UV-visible diffuse reflectance spectra where  $\text{BiVO}_4/\text{MnO}_2$  absorbed better than the pristine  $\text{BiVO}_4$  anode in the visible light region. This revealed that there was better charge separation in the heterostructured anode, and this was further established from the results obtained in the photoelectrochemical characterisation where the composite electrode gave a higher photocurrent response with a density of  $0.589 \text{ mA cm}^{-2}$  while  $\text{BiVO}_4$  gave only  $0.362 \text{ mA cm}^{-2}$ . The improved charge separation in the heterostructure photoanode resulted in 76% PEC removal of ciprofloxacin with a bias potential of 1.5 V under visible light irradiation within 2 h. In similar studies, a higher PEC removal of ciprofloxacin has also been recorded using  $\text{BiVO}_4/\text{BiOI}$  [96],  $\text{TiO}_2/\text{AgBiS}_2$  [97] and  $\text{BiVO}_4/\text{Ag}_2\text{S}$  [98] electrodes. The PEC degradation of antibiotic norfloxacin using nanostructured photoanodes with heterojunctions under solar light illuminations has also been reported [99,100].

Another category of recalcitrant organics that have been successfully degraded using nanostructured solar-responsive photoanodes consisting of heterojunctions is the phenols. For instance, Li et al. reported the PEC oxidation of 2–4 dichlorophenol using a photoanode of  $\text{Mo-BiVO}_4/\text{WO}_3$  heterojunction under visible light illumination [101]. The photoanode was prepared through a hydrothermal route and drop coating on FTO glass. The morphology of  $\text{Mo-BiVO}_4/\text{WO}_3$  as recorded with field emission scanning microscopy and revealed that the material was made of a nanoporous structure with worm-like nanoparticles having diameters in the range of 50–150 nm. The prepared heterostructured photoanode showed better absorption with a band edge of 505 nm in the visible light region than both pristine  $\text{WO}_3$  and  $\text{Mo-BiVO}_4$ . The  $\text{Mo-BiVO}_4/\text{WO}_3$  was employed as a photoanode to degrade 2,4-dichlorophenol with Pd/Ni acting as a photocathode. After 4 h, 2–4-dichlorophenol was hydro-dechlorinated to phenol and 45% of the phenol was mineralised after another 4 h. The mechanism of the reaction was proposed which suggested that the well-separated



photogenerated holes could be responsible for the degradation process as presented in Figure 5.

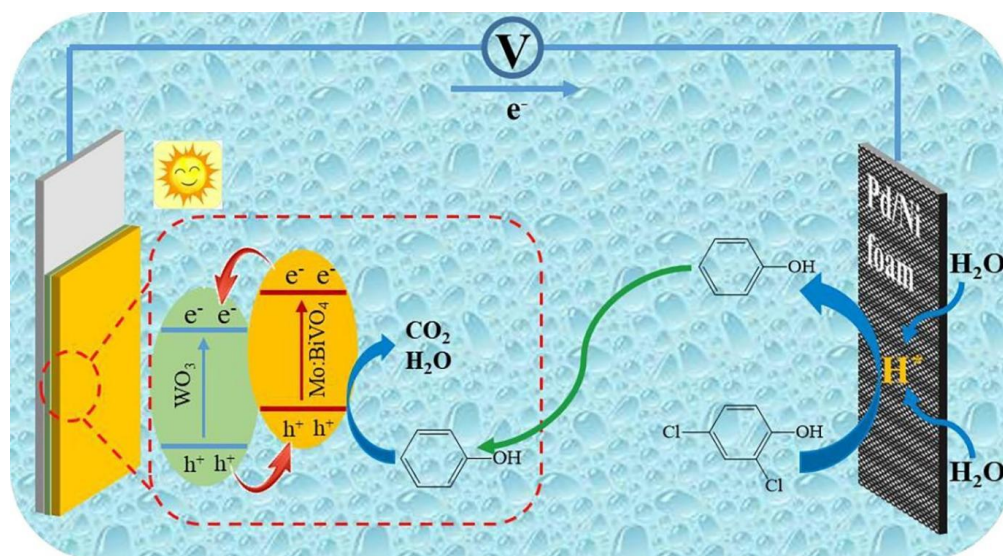


**Figure 5.** Mechanism of PEC degradation of 2,4 dichlorophenol using a Mo-BiVO<sub>4</sub>/WO<sub>3</sub> photoanode and Pd/Ni foam as a cathode. Reprinted/adapted with permission from Ref. [101]. Copyright 2019, Elsevier.

The reports of Wang et al. also confirmed the PEC degradation of phenols using a nanostructured photoanode with heterojunction [102]. The electrode consisted of a core-shell g-C<sub>3</sub>N<sub>4</sub>@ZnO which was prepared through the facile reflux technique. The morphological and structural results showed that ZnO nanoparticles and g-C<sub>3</sub>N<sub>4</sub> nanosheets were in the core-shell structure. The optical studies revealed that the incorporation of the g-C<sub>3</sub>N<sub>4</sub> shell into the ZnO core improved the visible light absorption of the ZnO nanoparticles. When the heterostructured photoanode was applied in the PEC degradation of phenol under visible light illumination, an impressive percentage removal of 97.3% was recorded in under 3 h which was significantly higher than what was obtained with the ZnO photoanode. The better PEC efficiency obtained was attributed to improving charge separation within the heterojunction interface. In another study, 99.9% PEC degradation of 2,4,6-trichlorophenol was achieved within 2 h with the use of Cu<sub>2</sub>O/TiO<sub>2</sub> nanotube arrays as a photoanode under visible light irradiation [103]. Indeed, much success has been recorded in the use of nanostructured photoanodes consisting of heterojunctions for PEC removal of organics. The better efficiencies achieved were due to efficient charge separations within the interface of the heterojunctions. Bisphenol A has also been successfully degraded through PEC using a heterostructured photoanode consisting of 2D TiO<sub>2</sub>/BiVO<sub>4</sub> nanostructures [104]. After 4 h, 80% degradation of bisphenol A was recorded, and the good PEC performance was due to the interparticle electron transport within the heterojunction. These results clearly showed that nanostructured photoanodes with a heterojunction are excellent materials for the degradation of a vast range of phenolic compounds.

Table 1 presents the summary of recent findings in the application of nanostructured materials as photoanodes in the PEC degradation of recalcitrant organic pollutants under solar light irradiation. The results showed that several kinds of modified and unmodified metal oxide nanomaterials are suitable for the remediation of wastewater through the PEC process.

**Table 1.** Nanostructured materials as photoanodes in PEC degradation of organic pollutants.

Photoanodes	Experimental Conditions	Results	Ref.
TiO <sub>2</sub>	Pollutant = norfloxacin; C <sub>0</sub> = 5 mg L <sup>−1</sup> ; SE = 0.5 M Na <sub>2</sub> SO <sub>4</sub> ; LS = 350 W Xe lamp	93% removal after 3 h	[40]
I-TiO <sub>2</sub>	Pollutant = diclofenac; C <sub>0</sub> = 0.1 M; SE = 0.1 M Na <sub>2</sub> SO <sub>4</sub> ; Bias potential = 1.4 V; LS = 400 W halogen lamp	99.4% removal after 2 h 60.2% TOC removal after 2 h	[41]
Fe <sup>3+</sup> -TiO <sub>2</sub>	Pollutant = bisphenol A; C <sub>0</sub> = 10 mg L <sup>−1</sup> ; SE = 0.1 M Na <sub>2</sub> SO <sub>4</sub> ; Current density = 1.25 mA cm <sup>−2</sup> ; LS = 150 W Xe lamp	82.59% removal after 4 h 73.8% TOC removal after 4 h	[42]
Fe-TiO <sub>2</sub>	Pollutant = methylene blue; C <sub>0</sub> = 10 mg L <sup>−1</sup> ; SE = 0.1 M K <sub>2</sub> SO <sub>4</sub> ; Potential = 1 V; LS = 500 W Xe lamp	98.79% removal after 2 h	[43]
Cs-TiO <sub>2</sub>	Pollutant = 4-chloroguaiacol; C <sub>0</sub> = 20 mg L <sup>−1</sup> ; SE = 160 mg L <sup>−1</sup> Na <sub>2</sub> SO <sub>4</sub> ; Current: 0.03 A	92% removal after 6 h	[44]
B-TiO <sub>2</sub>	Pollutant = propyphenazone; C <sub>0</sub> = 30 mg L <sup>−1</sup> ; SE = 0.05 M Na <sub>2</sub> SO <sub>4</sub> ; Potential = 1 V	94% removal after 2 h 18% TOC removal after 2 h	[47]
La, S, N—TiO <sub>2</sub>	Pollutant = benzene, toluene, xylene (BTX) solution; C <sub>0</sub> = 50 mg L <sup>−1</sup> ; SE = 0.1 M Na <sub>2</sub> SO <sub>4</sub> ; Potential = 0.8 V; LS = 400 W Osram lamp	83.7, 71.4, and 62.28% removal of benzene, toluene and xylene after 3 h	[48]
PPy—TiO <sub>2</sub>	Pollutant = methylene blue; C <sub>0</sub> = 10 mg L <sup>−1</sup> ; SE = 0.5 g L <sup>−1</sup> NaCl; Potential = 15 V; LS = 250 W Hg lamp	91.25% removal after 1 h	[53]
TiO <sub>2</sub> /PANI/PVDF	Pollutants = methylene blue and methyl orange; C <sub>0</sub> = 0.5 mg L <sup>−1</sup> ; Potential = 1 V; LS = 100 W Xe lamp	73.1% and 59.4% removal of methylene blue and methyl orange after 4 h	[54]
ZnO	Pollutants = methylene blue; C <sub>0</sub> = 5 mg L <sup>−1</sup> ; Potential = 1 V; LS = 100 W Xe lamp	71% removal after 1 h	[56]
Ni-ZnO	Pollutants = tetracycline; C <sub>0</sub> : 10 mg L <sup>−1</sup> ; Potential = 0.8 V; SE = 0.1 M Na <sub>2</sub> SO <sub>4</sub> ; LS = 300 W Xe lamp	87.5% removal after 3 h	[58]
Ni-ZnO	Pollutant = ciprofloxacin; C <sub>0</sub> = 5 mg L <sup>−1</sup> ; Current density = 1.87 mA cm <sup>−2</sup> ; SE = 0.75 g L <sup>−1</sup>	100% removal after 90 min 83.7% TOC removal after 90 min	[59]
Pd-ZnO	Pollutant = paracetamol; C <sub>0</sub> = 0.1 mM; Current density = 10 mA cm <sup>−2</sup> ; SE = 0.05 M Na <sub>2</sub> SO <sub>4</sub> ; LS = 150 W linear halogen lamp	100% removal after 3 h 71% TOC removal after 4 h	[61]
Ag@ZnO	Pollutant = rhodamine B; C <sub>0</sub> = 10 mg L <sup>−1</sup> ; Potential = 1.5 V; SE = 0.1 M Na <sub>2</sub> SO <sub>4</sub> ; LS = 500 W Xe lamp	82% removal after 2 h	[62]
WO <sub>3</sub>	Pollutant = brilliant blue; C <sub>0</sub> : 0.5 mM; Potential = 1.5 V; SE = 0.1 M Na <sub>2</sub> SO <sub>4</sub> ; LS = 100 W Xe lamp	85% COD removal after 4 h	[66]
WO <sub>3</sub>	Pollutant = fenamiphos; C <sub>0</sub> = 20 mg L <sup>−1</sup> ; Potential = 1 V; SE = 0.1 M Na <sub>2</sub> SO <sub>4</sub> ; LS = 100 W Xe lamp	100% removal after 2 h	[70]
Co-BiVO <sub>4</sub>	Pollutant = bisphenol A; C <sub>0</sub> = 20 mg L <sup>−1</sup> ; Potential = 1.2 V; SE = 2 mM peroxymonosulphate; LS = 300 W Xe lamp	99.16% removal after 1 h	[80]
TiO <sub>2</sub> /Ag <sub>3</sub> PO <sub>4</sub> /Ag <sub>4</sub> P <sub>2</sub> O <sub>7</sub>	Pollutant = methylene blue; C <sub>0</sub> = 10 mg L <sup>−1</sup> ; Potential = 0.5 V; SE = 0.2 M Na <sub>2</sub> SO <sub>4</sub> ; LS = 100 W Xe lamp	99.39% removal after 40 min	[86]
ZnO/MoS <sub>2</sub>	Pollutant = acid red 1; C <sub>0</sub> : 20 mg L <sup>−1</sup> ; Potential = 0.4 V; SE = 0.1 Na <sub>2</sub> SO <sub>4</sub> ; LS = 300 W Xe lamp	100% removal after 6 h	[87]
ZnO/BiVO <sub>4</sub>	Pollutant = tetracycline; C <sub>0</sub> = 20 mg L <sup>−1</sup> ; Potential = 1.2 V; SE = 0.1 M Na <sub>2</sub> SO <sub>4</sub> ; LS = 300 W Xe lamp	84.5% removal in 1 h	[93]
BiVO <sub>4</sub> /MnO <sub>2</sub>	Pollutant = ciprofloxacin; C <sub>0</sub> = 10 mg L <sup>−1</sup> ; Potential = 1.5 V; SE = 0.1 M Na <sub>2</sub> SO <sub>4</sub> ; LS = 100 W Xe lamp	76% removal in 2 h	[95]
BiVO <sub>4</sub> /Ag <sub>2</sub> S	Pollutant = sulphamethoxazole; C <sub>0</sub> = 10 mg L <sup>−1</sup> ; Potential = 1.2 V; SE = 0.1 M Na <sub>2</sub> SO <sub>4</sub> ; LS = 100 W Xe lamp	86% removal in 2 h	[98]
TiO <sub>2</sub> /g-C <sub>3</sub> N <sub>4</sub>	Pollutant = bisphenol A; C <sub>0</sub> = 10 mg L <sup>−1</sup> ; SE = 0.1 M Na <sub>2</sub> SO <sub>4</sub> ; Potential = 1.3 V; LS = 300 W Xe lamp	99.7% removal in 4 h	[104]

C<sub>0</sub>: initial concentration; SE: supporting electrolyte; PPy: polypyrrole.

## 2. Conclusions and Future Perspective

Remarkable progress has been made towards remediating the water environment through the adoption of novel wastewater treatment techniques for the removal of recalcitrant organic pollutants. The emergence of PEC degradation has led to outstanding success in the total mineralization of these organic pollutants. The PEC technique remains an attractive choice as a water treatment method because of its versatility, efficiency, easy operating setup, reduced energy cost and environmental friendliness. As observed, an easy way of improving the efficiency of semiconductor photocatalysts often used as photoanodes in PEC systems is by preparing them on a nanoscale with distinct morphology such as nanorods, nanowires, nanoplates, nanosheets or nanoparticles. This method has been effective since it improves the mobility of electrons within the nanostructures which results in better charge transfer.

Visible light active semiconductors such as  $\text{WO}_3$ ,  $\text{BiVO}_4$ ,  $\text{g-C}_3\text{N}_4$  and  $\text{Fe}_3\text{O}_4$  have been more employed as photoanodes when the source of irradiation intended for use is simulated sunlight which is mostly visible light radiation. However, most nanostructured metal oxide semiconductor photocatalysts employed as photoanodes in PEC degradation suffer the problem of rapid recombination of photoexcited electron-hole pairs which greatly impedes their PEC efficiency. Many attempts have been made to suppress this problem by doping the metal oxides with suitable metals or non-metals as well as coating them with conducting polymers such as polyaniline and polypyrroles. Another strategy is loading metal oxides with plasmonic transition metals such as silver and gold which help to reduce the spontaneous recombination of photogenerated charge carriers by acting as photosensitizers and through localized surface plasmon resonance effects. The results have confirmed these modifications greatly help to improve the solar light responsiveness of the photoanodes which consequently leads to better PEC degradation efficiencies when compared with their pristine counterparts.

In recent years, however, nanostructured semiconductor photoanodes consisting of heterojunction have been used for the degradation of pharmaceuticals, dyes and phenolic compounds. Heterostructured photoanodes have recorded higher PEC degradation efficiency than unitary semiconductor photoanodes. This is because heterojunction promotes efficient charge separation which results in the production of more reactive radicals which help to degrade organic compounds. It has been observed that semiconductors that perform poorly under visible light irradiation are often coupled with visible light-active semiconductors and the formed heterostructured anodes have been found to absorb photons better in the visible light region. The current trends reveal that scientists are using more heterostructured photoanodes in PEC wastewater treatment studies and this is due to their excellent PEC efficiency and ease of fabrication.

From the literature discussed, the following points should be addressed:

1. Most PEC degradation studies involving the use of nanostructured solar light-responsive photoanodes are often applied for the treatment of simulated wastewater on a laboratory scale. It is unfortunate that a large vacuum still exists in the literature concerning the real-life implementation of these photoanodes for the treatment of real wastewater effluents. Since the overall aim of developing the PEC degradation process is to remediate wastewater in the environment and make available cleaner water for use, it will be of more interest if future research focuses more on the treatment of real effluents either from industries or wastewater treatment plants. With this in view, researchers will endeavour to perform preliminary studies using a continuous flow process for PEC degradation rather than the batch process often use.
2. Additionally, the experimental conditions (such as analyte concentration) used to access the performance of materials in PEC degradation should be as close as possible to the conditions attainable in real-life situations.
3. It is also interesting to realise that the solar light responsiveness of the nanostructured photoanodes is often established through a series of experimental techniques in the laboratory whereas simulated solar light is commonly used as a light source for the

degradation process. Future research should endeavor to use direct sunlight as a source of illumination to excite these photoanodes as this will establish, without a doubt, the solar light responsiveness of these photoanodes.

Overall, it is evident that nanomaterials are excellent photoanodes for the PEC degradation of recalcitrant organics in aqueous solutions and there is a great prospect for their real-life applications for remediating polluted water in the near future.

**Author Contributions:** Conceptualization, B.O.O., A.O.I. and S.P.A.; methodology, B.O.O., A.O.I. and S.P.A.; software, B.O.O., A.O.I. and S.P.A.; validation, B.O.O., A.O.I. and S.P.A.; formal analysis, B.O.O., A.O.I., S.P.A. and S.A.; investigation, B.O.O., A.O.I., S.P.A., F.A.A. and S.A.; resources, S.A., M.M. and B.M.; data curation B.O.O. and A.O.I.; writing—original draft preparation, B.O.O., A.O.I. and S.P.A., F.A.A. and S.A.; writing—review and editing, B.O.O., A.O.I. and S.P.A.; visualization, S.A., M.M. and B.M.; supervision S.A., M.M. and B.M.; project administration, S.A., M.M. and B.M.; funding acquisition, S.A., M.M. and B.M. All authors have read and agreed to the published version of the manuscript.

**Funding:** This project was funded by the National Research Foundation (NRF), South Africa (grant number: 145431).

**Institutional Review Board Statement:** Not applicable.

**Informed Consent Statement:** Not applicable.

**Data Availability Statement:** Not applicable.

**Acknowledgments:** We acknowledged UNESCO-UNISA Africa Chair in Nanoscience and Nanotechnology College of Graduates Studies, University of South Africa, Pretoria 392, South Africa.

**Conflicts of Interest:** The authors declare no conflict of interest.

## References

1. Amoatey, P.; Baawain, M.S. Effects of pollution on freshwater aquatic organisms. *Water Environ. Res.* **2019**, *91*, 1272–1287. [[CrossRef](#)] [[PubMed](#)]
2. Wu, C.; Maurer, C.; Wang, Y.; Xue, S.; Davis, D.L. Water pollution and human health in China. *Environ. Health Perspect.* **1999**, *107*, 251–256. [[CrossRef](#)] [[PubMed](#)]
3. Rath, B.S.; Kumar, P.S.; Vo, D.-V.N. Critical review on hazardous pollutants in water environment: Occurrence, monitoring, fate, removal technologies and risk assessment. *Sci. Total Environ.* **2021**, *797*, 149134. [[CrossRef](#)] [[PubMed](#)]
4. Vasilachi, I.; Asimicesei, D.; Fertu, D.; Gavrilescu, M. Occurrence and Fate of Emerging Pollutants in Water Environment and Options for Their Removal. *Water* **2021**, *13*, 181. [[CrossRef](#)]
5. Serpone, N.; Artemev, Y.M.; Ryabchuk, V.K.; Emeline, A.V.; Horikoshi, S. Light-driven advanced oxidation processes in the disposal of emerging pharmaceutical contaminants in aqueous media: A brief review. *Curr. Opin. Green Sustain. Chem.* **2017**, *6*, 18–33. [[CrossRef](#)]
6. Mompelat, S.; Le Bot, B.; Thomas, O. Occurrence and fate of pharmaceutical products and by-products, from resource to drinking water. *Environ. Int.* **2009**, *35*, 803–814. [[CrossRef](#)]
7. Mondal, S.K.; Saha, A.K.; Sinha, A. Removal of ciprofloxacin using modified advanced oxidation processes: Kinetics, pathways and process optimization. *J. Clean. Prod.* **2018**, *171*, 1203–1214. [[CrossRef](#)]
8. Vălitalo, P.; Kruglova, A.; Mikola, A.; Vahala, R. Toxicological impacts of antibiotics on aquatic micro-organisms: A mini-review. *Int. J. Hyg. Environ. Health* **2017**, *220*, 558–569. [[CrossRef](#)]
9. Zwane, B.N.; Orimolade, B.O.; Koiki, B.A.; Mabuba, N.; Gomri, C.; Petit, E.; Bonniol, V.; Lesage, G.; Rivallin, M.; Cretin, M.; et al. Combined Electro-Fenton and Anodic Oxidation Processes at a Sub-Stoichiometric Titanium Oxide (Ti<sub>4</sub>O<sub>7</sub>) Ceramic Electrode for the Degradation of Tetracycline in Water. *Water* **2021**, *13*, 2772. [[CrossRef](#)]
10. Saafie, N.; Zulfiqar, M.; Samsudin, M.F.R.; Sufian, S. Current Scenario of MXene-Based Nanomaterials for Wastewater Remediation: A Review. *Chemistry* **2022**, *4*, 1576–1608. [[CrossRef](#)]
11. Ahmed, S.F.; Mofijur, M.; Ahmed, B.; Mehnaz, T.; Mehejabin, F.; Malat, D.; Hoang, A.T.; Shafiullah, G.M. Nanomaterials as a sustainable choice for treating wastewater. *Environ. Res.* **2022**, *214*, 113807. [[CrossRef](#)] [[PubMed](#)]
12. Palani, G.; Arputhalatha, A.; Kannan, K.; Lakkaboyana, S.K.; Hanafiah, M.M.; Kumar, V.; Marella, R.K. Current Trends in the Application of Nanomaterials for the Removal of Pollutants from Industrial Wastewater Treatment—A Review. *Molecules* **2021**, *26*, 2799. [[CrossRef](#)]
13. Wu, Y.; Pang, H.; Liu, Y.; Wang, X.; Yu, S.; Fu, D.; Chen, J.; Wang, X. Environmental remediation of heavy metal ions by novel-nanomaterials: A review. *Environ. Pollut.* **2019**, *246*, 608–620. [[CrossRef](#)]



14. Santhosh, C.; Velmurugan, V.; Jacob, G.; Jeong, S.K.; Grace, A.N.; Bhatnagar, A. Role of nanomaterials in water treatment applications: A review. *Chem. Eng. J.* **2016**, *306*, 1116–1137. [\[CrossRef\]](#)
15. Bethi, B.; Sonawane, S.H.; Bhanvase, B.A.; Gumfekar, S.P. Nanomaterials-based advanced oxidation processes for wastewater treatment: A review. *Chem. Eng. Process. Process Intensif.* **2016**, *109*, 178–189. [\[CrossRef\]](#)
16. Teow, Y.H.; Mohammad, A.W. New generation nanomaterials for water desalination: A review. *Desalination* **2019**, *451*, 2–17. [\[CrossRef\]](#)
17. Gontarek-Castro, E.; Castro-Muñoz, R.; Lieder, M. New insights of nanomaterials usage toward superhydrophobic membranes for water desalination via membrane distillation: A review. *Crit. Rev. Environ. Sci. Technol.* **2022**, *52*, 2104–2149. [\[CrossRef\]](#)
18. Daneshkhah, M.; Hossaini, H.; Malakootian, M. Removal of metoprolol from water by sepiolite-supported nanoscale zero-valent iron. *J. Environ. Chem. Eng.* **2017**, *5*, 3490–3499. [\[CrossRef\]](#)
19. Velepini, T.; Prabakaran, E.; Pillay, K. Recent developments in the use of metal oxides for photocatalytic degradation of pharmaceutical pollutants in water—A review. *Mater. Today Chem.* **2021**, *19*, 100380. [\[CrossRef\]](#)
20. Deegan, A.M.; Shaik, B.; Nolan, K.; Urell, K.; Oelgemöller, M.; Tobin, J.; Morrissey, A. Treatment options for wastewater effluents from pharmaceutical companies. *Int. J. Environ. Sci. Technol.* **2011**, *8*, 649–666. [\[CrossRef\]](#)
21. Sirés, I.; Brillas, E.; Oturan, M.A.; Rodrigo, M.A.; Panizza, M. Electrochemical advanced oxidation processes: Today and tomorrow. A review. *Environ. Sci. Pollut. Res.* **2014**, *21*, 8336–8367. [\[CrossRef\]](#) [\[PubMed\]](#)
22. Peleyeju, M.G.; Arotiba, O.A. Recent trend in visible-light photoelectrocatalytic systems for degradation of organic contaminants in water/wastewater. *Environ. Sci. Water Res. Technol.* **2018**, *4*, 1389–1411. [\[CrossRef\]](#)
23. Zarei, E.; Ojani, R. Fundamentals and some applications of photoelectrocatalysis and effective factors on its efficiency: A review. *J. Solid State Electrochem.* **2017**, *21*, 305–336. [\[CrossRef\]](#)
24. Garcia-Segura, S.; Brillas, E. Applied photoelectrocatalysis on the degradation of organic pollutants in wastewaters. *J. Photochem. Photobiol. C Photochem. Rev.* **2017**, *31*, 1–35. [\[CrossRef\]](#)
25. Oturan, M.A.; Aaron, J.J. Advanced oxidation processes in water/wastewater treatment: Principles and applications. A review. *Crit. Rev. Environ. Sci. Technol.* **2014**, *44*, 2577–2641. [\[CrossRef\]](#)
26. Peleyeju, M.G.; Umukoro, E.H.; Tshwenya, L.; Moutloali, R.; Babalola, J.O.; Arotiba, O.A. Photoelectrocatalytic water treatment systems: Degradation, kinetics and intermediate products studies of sulfamethoxazole on a TiO<sub>2</sub>-exfoliated graphite electrode. *RSC Adv.* **2017**, *7*, 40571–40580. [\[CrossRef\]](#)
27. Wu, S.; Hu, Y.H. A comprehensive review on catalysts for electrocatalytic and photoelectrocatalytic degradation of antibiotics. *Chem. Eng. J.* **2021**, *409*, 127739. [\[CrossRef\]](#)
28. Daghrir, R.; Drogui, P.; Robert, D. Photoelectrocatalytic technologies for environmental applications. *J. Photochem. Photobiol. A Chem.* **2012**, *238*, 41–52. [\[CrossRef\]](#)
29. Yusuf, T.L.; Orimolade, B.O.; Masekela, D.; Mamba, B.; Mabuba, N. The application of photoelectrocatalysis in the degradation of rhodamine B in aqueous solutions: A review. *RSC Adv.* **2022**, *12*, 26176–26191. [\[CrossRef\]](#)
30. Sirés, I.; Brillas, E. Remediation of water pollution caused by pharmaceutical residues based on electrochemical separation and degradation technologies: A review. *Environ. Int.* **2012**, *40*, 212–229. [\[CrossRef\]](#)
31. Liu, Y.; Gan, X.; Zhou, B.; Xiong, B.; Li, J.; Dong, C.; Bai, J.; Cai, W. Photoelectrocatalytic degradation of tetracycline by highly effective TiO<sub>2</sub> nanopore arrays electrode. *J. Hazard. Mater.* **2009**, *171*, 678–683. [\[CrossRef\]](#) [\[PubMed\]](#)
32. Zhang, Y.; Xiong, X.; Han, X.; Zhang, X.; Shen, F.; Deng, S.; Xiao, H.; Yang, X.; Yang, G.; Peng, H. Photoelectrocatalytic degradation of recalcitrant organic pollutants using TiO<sub>2</sub> film electrodes: An overview. *Chemosphere* **2012**, *88*, 145–154. [\[CrossRef\]](#)
33. Martins, A.S.; Cordeiro-Junior, P.J.M.; Bessegato, G.G.; Carneiro, J.F.; Zanon, M.V.B.; de Vasconcelos Lanza, M.R. Electrodeposition of WO<sub>3</sub> on Ti substrate and the influence of interfacial oxide layer generated in situ: A photoelectrocatalytic degradation of propyl paraben. *Appl. Surf. Sci.* **2019**, *464*, 664–672. [\[CrossRef\]](#)
34. Li, R.; Zhao, X.; Chen, X.; Jiang, T.; Leung, D.Y.C.; Pan, D.; Li, G.; Wang, W. g-C<sub>3</sub>N<sub>4</sub> photoanode for photoelectrocatalytic synergistic pollutant degradation and hydrogen evolution. *Appl. Surf. Sci.* **2018**, *467–468*, 658–665. [\[CrossRef\]](#)
35. Zhang, M.; Pu, W.; Pan, S.; Okoth, O.K.; Yang, C.; Zhang, J. Photoelectrocatalytic activity of liquid phase deposited  $\alpha$ -Fe<sub>2</sub>O<sub>3</sub> films under visible light illumination. *J. Alloys Compd.* **2015**, *648*, 719–725. [\[CrossRef\]](#)
36. Zhou, Y.; Fan, X.; Zhang, G.; Dong, W. Fabricating MoS<sub>2</sub> nanoflakes photoanode with unprecedented high photoelectrochemical performance and multi-pollutants degradation test for water treatment. *Chem. Eng. J.* **2019**, *356*, 1003–1013. [\[CrossRef\]](#)
37. Orimolade, B.O.; Arotiba, O.A. An Exfoliated Graphite-Bismuth Vanadate Composite Photoanode for the Photoelectrochemical Degradation of Acid Orange 7 Dye. *Electrocatalysis* **2019**, *10*, 429–435. [\[CrossRef\]](#)
38. Orimolade, B.O.; Idris, A.O.; Feleni, U.; Mamba, B. Peroxymonosulfate assisted photoelectrocatalytic degradation of pharmaceuticals at a FTO-Bi<sub>2</sub>WO<sub>6</sub> electrode: Mechanism and kinetics studies. *Catal. Commun.* **2022**, *169*, 106481. [\[CrossRef\]](#)
39. Yao, T.; An, X.; Han, H.; Chen, J.Q.; Li, C. Photoelectrocatalytic Materials for Solar Water Splitting. *Adv. Energy Mater.* **2018**, *8*, 1800210. [\[CrossRef\]](#)
40. Zhang, X.; Li, D.; Wan, J.; Yu, X. Hydrothermal synthesis of TiO<sub>2</sub> nanosheets photoelectrocatalyst on Ti mesh for degradation of norfloxacin: Influence of pickling agents. *Mater. Sci. Semicond. Process.* **2016**, *43*, 47–54. [\[CrossRef\]](#)
41. Liu, D.; Wang, J.; Zhou, J.; Xi, Q.; Li, X.; Nie, E.; Piao, X.; Sun, Z. Fabricating I doped TiO<sub>2</sub> photoelectrode for the degradation of diclofenac: Performance and mechanism study. *Chem. Eng. J.* **2019**, *369*, 968–978. [\[CrossRef\]](#)



42. Xiang, G.; Yu, Z.; Hou, Y.; Chen, Y.; Peng, Z.; Sun, L.; Sun, L. Simulated solar-light induced photoelectrocatalytic degradation of bisphenol-A using Fe<sub>3</sub>+doped TiO<sub>2</sub> nanotube arrays as a photoanode with simultaneous aeration. *Sep. Purif. Technol.* **2016**, *161*, 144–151. [\[CrossRef\]](#)
43. Wang, Q.; Jin, R.; Zhang, M.; Gao, S. Solvothermal preparation of Fe-doped TiO<sub>2</sub> nanotube arrays for enhancement in visible light induced photoelectrochemical performance. *J. Alloys Compd.* **2017**, *690*, 139–144. [\[CrossRef\]](#)
44. Rajput, H.; Changotra, R.; Kumar, V.; Kumar, S.; Dhir, A. Chemosphere A facile synthesis of Cs loaded TiO<sub>2</sub> nanotube photoelectrode for the removal of 4-chloroguaiacol. *Chemosphere* **2019**, *218*, 687–695. [\[CrossRef\]](#) [\[PubMed\]](#)
45. Cui, Y.; Deng, X.; Ma, Q.; Zhang, H.; Cheng, X.; Li, X.; Xie, M.; Cheng, Q.; Li, B. Kinetics of photoelectrocatalytic degradation of diclofenac using N, S CO-doped TiO<sub>2</sub> nano-crystallite decorated TiO<sub>2</sub> nanotube arrays photoelectrode. *Environ. Prot. Eng.* **2018**, *44*, 117–130. [\[CrossRef\]](#)
46. Liu, D.; Zhou, J.; Wang, J.; Tian, R.; Li, X.; Nie, E.; Piao, X.; Sun, Z. Enhanced visible light photoelectrocatalytic degradation of organic contaminants by F and Sn co-doped TiO<sub>2</sub> photoelectrode. *Chem. Eng. J.* **2018**, *344*, 332–341. [\[CrossRef\]](#)
47. Da Silva, T.F.; Cavalcante, R.P.; Guelfi, D.R.V.; de Oliveira, S.C.; Casagrande, G.A.; Caires, A.R.L.; de Oliveira, F.F.; Gubiani, J.R.; Cardoso, J.C.; Machulek, A. Photo-anodes based on B-doped TiO<sub>2</sub> for photoelectrocatalytic degradation of propyphenazone: Identification of intermediates, and acute toxicity evaluation. *J. Environ. Chem. Eng.* **2022**, *10*, 107212. [\[CrossRef\]](#)
48. Ghanbarnezhad, M.; Parvareh, A.; Keshavarz Moraveji, M.; Jorfi, S. La, S, N tri-doped TiO<sub>2</sub>/nickel foam as efficient photoelectrode for degradation of BTX solution under visible light irradiation. *J. Photochem. Photobiol. A Chem.* **2022**, *431*, 114044. [\[CrossRef\]](#)
49. Yin, Y.; Liu, E.; Li, H.; Wan, J.; Fan, J.; Hu, X.; Li, J.; Tang, C.; Pu, C. Fabrication of plasmonic Au/TiO<sub>2</sub> nanotube arrays with enhanced photoelectrocatalytic activities. *Ceram. Int.* **2016**, *42*, 9387–9395. [\[CrossRef\]](#)
50. Wang, Q.; Wang, X.; Zhang, M.; Li, G.; Gao, S.; Li, M.; Zhang, Y. Influence of Ag-Au microstructure on the photoelectrocatalytic performance of TiO<sub>2</sub> nanotube array photocatalysts. *J. Colloid Interface Sci.* **2016**, *463*, 308–316. [\[CrossRef\]](#) [\[PubMed\]](#)
51. Chen, Z.; Yang, J.; Yang, X.; Zhao, Y.; Kang, J.; Yang, F.; Zhang, Y.; Cheng, M.; Wang, G.; Duanmu, Q. Porous Si/TiO<sub>2</sub> nanowire photoanode for photoelectric catalysis under simulated solar light irradiation. *Appl. Organomet. Chem.* **2018**, *32*, 2–10. [\[CrossRef\]](#)
52. Wang, H.; Han, B.; Lu, J.; Wu, P.; Cui, W. Excellent photoelectrocatalytic degradation and superior charge separation of polyaniline nanosheets wrapped TiO<sub>2</sub> nanotube arrays. *Mater. Lett.* **2020**, *260*, 126906. [\[CrossRef\]](#)
53. Zhang, J.; Pang, Z.; Sun, Q.; Chen, X.; Zhu, Y.; Li, M.; Wang, J.; Qiu, H.; Li, X.; Li, Y.; et al. TiO<sub>2</sub> nanotube array modified with polypyrrole for efficient photoelectrocatalytic decolorization of methylene blue. *J. Alloys Compd.* **2020**, *820*, 153128. [\[CrossRef\]](#)
54. Sboui, M.; Niu, W.; Li, D.; Lu, G.; Zhou, N.; Zhang, K.; Pan, J.H. Fabrication of electrically conductive TiO<sub>2</sub>/PANI/PVDF composite membranes for simultaneous photoelectrocatalysis and microfiltration of azo dye from wastewater. *Appl. Catal. A Gen.* **2022**, *644*, 118837. [\[CrossRef\]](#)
55. Fan, M.; Yang, C.; Pu, W.; Zhang, J. Liquid phase deposition of ZnO film for photoelectrocatalytic degradation of p-nitrophenol. *Mater. Sci. Semicond. Process.* **2014**, *17*, 104–109. [\[CrossRef\]](#)
56. Lunkham, C.; Ngerchuklin, P.; Ponchio, C. Photoelectrocatalytic and ultrasonic-assisted effects for organic dye degradation using zinc oxide (ZnO) electrode. *Key Eng. Mater.* **2019**, *798*, 404–411. [\[CrossRef\]](#)
57. Hunge, Y.M.; Yadav, A.A.; Kulkarni, S.B.; Mathe, V.L. A multifunctional ZnO thin film based devices for photoelectrocatalytic degradation of terephthalic acid and CO<sub>2</sub> gas sensing applications. *Sens. Actuators B Chem.* **2018**, *274*, 1–9. [\[CrossRef\]](#)
58. Feng, J.; Tian, Y.; Okoth, O.K.; Cheng, L.; Zhang, J. Liquid Phase Deposition of Nickel-Doped ZnO Film with Enhanced Visible Light Photoelectrocatalytic Activity. *J. Electrochem. Soc.* **2019**, *166*, H685–H690. [\[CrossRef\]](#)
59. Hosseini, M.; Esrafil, A.; Farzadkia, M.; Kermani, M.; Gholami, M. Degradation of ciprofloxacin antibiotic using photoelectrocatalyst process of Ni-doped ZnO deposited by RF sputtering on FTO as an anode electrode from aquatic environments: Synthesis, kinetics, and ecotoxicity study. *Microchem. J.* **2020**, *154*, 104663. [\[CrossRef\]](#)
60. Gholami, M.; Rasoulzadeh, H.; Ahmadi, T.; Hosseini, M. Synthesis, characterization of Nickel doped Zinc oxide by radio-frequency sputtering and application in photo-electrocatalysis degradation of Norfloxacin. *Mater. Lett.* **2020**, *269*, 127647. [\[CrossRef\]](#)
61. Nada, A.A.; Orimolade, B.O.; El-maghrabi, H.H.; Koiki, B.A.; Rivallin, M.; Bekheet, M.F.; Viter, R.; Damberga, D.; Lesage, G.; Iatsunskyi, I.; et al. Photoelectrocatalysis of paracetamol on Pd–ZnO/N-doped carbon nanofibers electrode. *Appl. Mater. Today* **2021**, *24*, 101129. [\[CrossRef\]](#)
62. Trang, T.N.Q.; Phan, T.B.; Nam, N.D.; Thu, V.T.H. In Situ Charge Transfer at the Ag@ZnO Photoelectrochemical Interface toward the High Photocatalytic Performance of H<sub>2</sub> Evolution and RhB Degradation. *ACS Appl. Mater. Interfaces* **2020**, *12*, 12195–12206. [\[CrossRef\]](#) [\[PubMed\]](#)
63. Tian, Y.; Cheng, L.; Zhang, J. Fabrication of Co-doped ZnO photoanode by liquid phase deposition for photoelectrocatalytic degradation of ofloxacin under visible light. *J. Electrochem. Soc.* **2018**, *165*, H284–H290. [\[CrossRef\]](#)
64. Li, Y.; Tang, Z.; Zhang, J.; Zhang, Z. Enhanced photocatalytic performance of tungsten oxide through tuning exposed facets and introducing oxygen vacancies. *J. Alloys Compd.* **2017**, *708*, 358–366. [\[CrossRef\]](#)
65. Zeng, Q.; Li, J.; Bai, J.; Li, X.; Xia, L.; Zhou, B. Preparation of vertically aligned WO<sub>3</sub> nanoplate array films based on peroxotungstate reduction reaction and their excellent photoelectrocatalytic performance. *Appl. Catal. B Environ.* **2017**, *202*, 388–396. [\[CrossRef\]](#)
66. Hunge, Y.M.; Yadav, A.A.; Mahadik, M.A.; Mathe, V.L.; Bhosale, C.H. A highly efficient visible-light responsive sprayed WO<sub>3</sub>/FTO photoanode for photoelectrocatalytic degradation of brilliant blue. *J. Taiwan Inst. Chem. Eng.* **2018**, *85*, 273–281. [\[CrossRef\]](#)

67. Hunge, Y.M.; Mahadik, M.A.; Mohite, V.S.; Kumbhar, S.S.; Deshpande, N.G.; Rajpure, K.Y.; Moholkar, A.V.; Patil, P.S.; Bhosale, C.H. Photoelectrocatalytic degradation of methyl blue using sprayed WO<sub>3</sub> thin films. *J. Mater. Sci. Mater. Electron.* **2016**, *27*, 1629–1635. [\[CrossRef\]](#)
68. Mohite, S.V.; Ganbavle, V.V.; Rajpure, K.Y. Solar photoelectrocatalytic activities of rhodamine-B using sprayed WO<sub>3</sub> photoelectrode. *J. Alloys Compd.* **2016**, *655*, 106–113. [\[CrossRef\]](#)
69. Fernández-Domene, R.M.; Sánchez-Tovar, R.; Lucas-Granados, B.; Muñoz-Portero, M.J.; Ramírez-Grau, R.; García-Antón, J. Visible-light photoelectrodegradation of diuron on WO<sub>3</sub> nanostructures. *J. Environ. Manag.* **2018**, *226*, 249–255. [\[CrossRef\]](#)
70. Roselló-Márquez, G.; Fernández-Domene, R.M.; Sánchez-Tovar, R.; García-Antón, J. Photoelectrocatalyzed degradation of organophosphorus pesticide fenamiphos using WO<sub>3</sub> nanorods as photoanode. *Chemosphere* **2020**, *246*, 125677. [\[CrossRef\]](#)
71. Roselló-Márquez, G.; Fernández-Domene, R.M.; García-Antón, J. Organophosphorus pesticides (chlorfenvinphos, phosmet and fenamiphos) photoelectrodegradation by using WO<sub>3</sub> nanostructures as photoanode. *J. Electroanal. Chem.* **2021**, *894*, 115366. [\[CrossRef\]](#)
72. Roselló-Márquez, G.; Fernández-Domene, R.M.; Sánchez-Tovar, R.; García-Carrión, S.; Lucas-Granados, B.; García-Antón, J. Photoelectrocatalyzed degradation of a pesticides mixture solution (chlorfenvinphos and bromacil) by WO<sub>3</sub> nanosheets. *Sci. Total Environ.* **2019**, *674*, 88–95. [\[CrossRef\]](#) [\[PubMed\]](#)
73. Mohite, S.V.; Ganbavle, V.V.; Rajpure, K.Y. Photoelectrochemical performance and photoelectrocatalytic degradation of organic compounds using Ga:WO<sub>3</sub> thin films. *J. Photochem. Photobiol. A Chem.* **2017**, *344*, 56–63. [\[CrossRef\]](#)
74. Liu, Y.; Li, Y.; Li, W.; Han, S.; Liu, C. Photoelectrochemical properties and photocatalytic activity of nitrogen-doped nanoporous WO<sub>3</sub> photoelectrodes under visible light. *Appl. Surf. Sci.* **2012**, *258*, 5038–5045. [\[CrossRef\]](#)
75. Umukoro, E.H.; Peleyeju, M.G.; Ngila, J.C.; Arotiba, O.A. Towards wastewater treatment: Photo-assisted electrochemical degradation of 2-nitrophenol and orange II dye at a tungsten trioxide-exfoliated graphite composite electrode. *Chem. Eng. J.* **2017**, *317*, 290–301. [\[CrossRef\]](#)
76. Luan, P.; Zhang, J. Stepping towards Solar Water Splitting: Recent Progress in Bismuth Vanadate Photoanodes. *ChemElectroChem* **2019**, *6*, 3227–3243. [\[CrossRef\]](#)
77. Deshpande, N.G.; Ahn, C.H.; Koli, R.R.; Jamadar, A.S.; Kim, D.S.; Kim, Y.B.; Jung, S.H.; Cho, H.K. Controlled nanostructured morphology of BiVO<sub>4</sub> photoanodes for efficient on-demand catalysis in solar water-splitting and sustainable water-treatment. *Appl. Surf. Sci.* **2020**, *514*, 146075. [\[CrossRef\]](#)
78. Xia, L.; Chen, F.; Li, J.; Chen, S.; Bai, J.; Zhou, T.; Li, L.; Xu, Q.; Zhou, B. Efficient organic pollutants conversion and electricity generation for carbonate-containing wastewater based on carbonate radical reactions initiated by BiVO<sub>4</sub>-Au/PVC system. *J. Hazard. Mater.* **2020**, *389*, 122140. [\[CrossRef\]](#)
79. Bacha, A.U.R.; Cheng, H.; Han, J.; Nabi, I.; Li, K.; Wang, T.; Yang, Y.; Ajmal, S.; Liu, Y.; Zhang, L. Significantly accelerated PEC degradation of organic pollutant with addition of sulfite and mechanism study. *Appl. Catal. B Environ.* **2019**, *248*, 441–449. [\[CrossRef\]](#)
80. Bacha, A.U.R.; Nabi, I.; Cheng, H.; Li, K.; Ajmal, S.; Wang, T.; Zhang, L. Photoelectrocatalytic degradation of endocrine-disruptor bisphenol—A with significantly activated peroxymonosulfate by Co-BiVO<sub>4</sub> photoanode. *Chem. Eng. J.* **2020**, *389*, 124482. [\[CrossRef\]](#)
81. Wang, S.; Yun, J.H.; Luo, B.; Butburee, T.; Peerakiatkhajohn, P.; Thaweesak, S.; Xiao, M.; Wang, L. Recent Progress on Visible Light Responsive Heterojunctions for Photocatalytic Applications. *J. Mater. Sci. Technol.* **2017**, *33*, 1–22. [\[CrossRef\]](#)
82. Zhang, L.; Jaroniec, M. Toward designing semiconductor-semiconductor heterojunctions for photocatalytic applications. *Appl. Surf. Sci.* **2018**, *430*, 2–17. [\[CrossRef\]](#)
83. Low, J.; Yu, J.; Jaroniec, M.; Wageh, S.; Al-Ghamdi, A.A. Heterojunction Photocatalysts. *Adv. Mater.* **2017**, *29*, 1601694. [\[CrossRef\]](#)
84. Low, J.; Jiang, C.; Cheng, B.; Wageh, S.; Al-Ghamdi, A.A.; Yu, J. A Review of Direct Z-Scheme Photocatalysts. *Small Methods* **2017**, *1*, 1700080. [\[CrossRef\]](#)
85. Arotiba, O.A.; Orimolade, B.O.; Koiki, B.A. Visible Light Driven Photoelectrocatalytic Semiconductor Heterojunction Anodes for Water Treatment Applications. *Curr. Opin. Electrochem.* **2020**, *22*, 25–34. [\[CrossRef\]](#)
86. Qiu, L.; Cui, Y.; Tan, X.; Zheng, S.; Zhang, H.; Xu, J.; Wang, Q. Construction of Ag<sub>3</sub>PO<sub>4</sub>/Ag<sub>4</sub>P<sub>2</sub>O<sub>7</sub> nanospheres sensitized hierarchical titanium dioxide nanotube mesh for photoelectrocatalytic degradation of methylene blue. *Sep. Purif. Technol.* **2019**, *215*, 619–624. [\[CrossRef\]](#)
87. Fei, W.; Li, H.; Li, N.; Chen, D.; Xu, Q.; Li, H.; He, J.; Lu, J. Facile fabrication of ZnO/MoS<sub>2</sub> p-n junctions on Ni foam for efficient degradation of organic pollutants through photoelectrocatalytic process. *Sol. Energy* **2020**, *199*, 164–172. [\[CrossRef\]](#)
88. Orimolade, B.O.; Koiki, B.A.; Zwane, B.N.; Peleyeju, G.M.; Mabuba, N.; Arotiba, O.A. Interrogating solar photoelectrocatalysis on an exfoliated graphite-BiVO<sub>4</sub>/ZnO composite electrode towards water treatment. *RSC Adv.* **2019**, *9*, 16586–16595. [\[CrossRef\]](#)
89. Ma, M.; Lei, E.; Zhao, D.; Xin, Y.; Wu, X.; Meng, Y.; Liu, Z. The p-n heterojunction of BiVO<sub>4</sub>/Cu<sub>2</sub>O was decorated by plasma Ag NPs for efficient photoelectrochemical degradation of Rhodamine B. *Colloids Surf. A Physicochem. Eng. Asp.* **2022**, *633*, 127834. [\[CrossRef\]](#)
90. Ma, Q.; Zhang, H.; Guo, R.; Li, B.; Zhang, X.; Cheng, X.; Xie, M.; Cheng, Q. Construction of CuS/TiO<sub>2</sub> nano-tube arrays photoelectrode and its enhanced visible light photoelectrocatalytic decomposition and mechanism of penicillin G. *Electrochim. Acta* **2018**, *283*, 1154–1162. [\[CrossRef\]](#)

91. Adhikari, S.; Selvaraj, S.; Kim, D.H. Construction of heterojunction photoelectrode via atomic layer deposition of  $\text{Fe}_2\text{O}_3$  on  $\text{Bi}_2\text{WO}_6$  for highly efficient photoelectrochemical sensing and degradation of tetracycline. *Appl. Catal. B Environ.* **2019**, *244*, 11–24. [\[CrossRef\]](#)
92. Feng, J.; Cheng, L.; Zhang, J.; Okoth, O.K.; Chen, F. Preparation of  $\text{BiVO}_4/\text{ZnO}$  composite film with enhanced visible-light photoelectrocatalytic activity. *Ceram. Int.* **2018**, *44*, 3672–3677. [\[CrossRef\]](#)
93. Li, Y.; Sun, X.; Tang, Y.; Ng, Y.H.; Li, L.; Jiang, F.; Wang, J.; Chen, W.; Li, L. Understanding photoelectrocatalytic degradation of tetracycline over three-dimensional coral-like  $\text{ZnO}/\text{BiVO}_4$  nanocomposite. *Mater. Chem. Phys.* **2021**, *271*, 124871. [\[CrossRef\]](#)
94. Orimolade, B.O.; Idris, A.O.; Feleni, U.; Mamba, B. Enhanced visible light driven photoelectrochemical degradation of tetracycline hydrochloride using a  $\text{BiOI}$  photoanode modified with  $\text{MnO}_2$  films. *Environ. Sci. Pollut. Res.* **2022**, *29*, 92530. [\[CrossRef\]](#) [\[PubMed\]](#)
95. Orimolade, B.O.; Zwane, B.N.; Koiki, B.A.; Tshwenya, L.; Peleyeju, G.M.; Mabuba, N.; Zhou, M.; Arotiba, O.A. Solar photoelectrocatalytic degradation of ciprofloxacin at a  $\text{FTO}/\text{BiVO}_4/\text{MnO}_2$  anode: Kinetics, intermediate products and degradation pathway studies. *J. Environ. Chem. Eng.* **2020**, *8*, 103607. [\[CrossRef\]](#)
96. Orimolade, B.O.; Koiki, B.A.; Peleyeju, G.M.; Arotiba, O.A. Visible light driven photoelectrocatalysis on a  $\text{FTO}/\text{BiVO}_4/\text{BiOI}$  anode for water treatment involving emerging pharmaceutical pollutants. *Electrochim. Acta* **2019**, *307*, 285–292. [\[CrossRef\]](#)
97. Parsaei-Khomami, A.; Mousavi, M.; Habibi, M.M.; Shirzad, K.; Ghasemi, J.B.; Wang, L.; Yu, J.; Yu, H.; Li, X. Highly efficient visible light photoelectrochemical degradation of ciprofloxacin and azo dyes by novel  $\text{TiO}_2/\text{AgBiS}_2$  photoelectrocatalyst. *Solid State Sci.* **2022**, *134*, 107044. [\[CrossRef\]](#)
98. Orimolade, B.O.; Arotiba, O.A. Towards visible light driven photoelectrocatalysis for water treatment: Application of a  $\text{FTO}/\text{BiVO}_4/\text{Ag}_2\text{S}$  heterojunction anode for the removal of emerging pharmaceutical pollutants. *Sci. Rep.* **2020**, *10*, 5348. [\[CrossRef\]](#) [\[PubMed\]](#)
99. Cao, D.; Wang, Y.; Qiao, M.; Zhao, X. Enhanced photoelectrocatalytic degradation of norfloxacin by an  $\text{Ag}_3\text{PO}_4/\text{BiVO}_4$  electrode with low bias. *J. Catal.* **2018**, *360*, 240–249. [\[CrossRef\]](#)
100. Du, H.; Pu, W.; Wang, Y.; Yan, K.; Feng, J.; Zhang, J.; Yang, C.; Gong, J. Synthesis of  $\text{BiVO}_4/\text{WO}_3$  composite film for highly efficient visible light induced photoelectrocatalytic oxidation of norfloxacin. *J. Alloys Compd.* **2019**, *787*, 284–294. [\[CrossRef\]](#)
101. Li, K.; Yang, Y.; Bacha, A.U.R.; Feng, Y.; Ajmal, S.; Nabi, I.; Zhang, L. Efficiently complete degradation of 2,4-DCP using sustainable photoelectrochemical reduction and sequential oxidation method. *Chem. Eng. J.* **2019**, *378*, 122191. [\[CrossRef\]](#)
102. Wei, W.; Zhu, Y.; Wang, J.; Chen, X.; Yao, W.; Gao, X.; Zong, R.; Yang, Z. Core-shell  $\text{g-C}_3\text{N}_4/\text{ZnO}$  composites as photoanodes with double synergistic effects for enhanced visible-light photoelectrocatalytic activities. *Appl. Catal. B Environ.* **2017**, *217*, 169–180. [\[CrossRef\]](#)
103. Ma, Q.; Zhang, H.; Cui, Y.; Deng, X.; Guo, R.; Cheng, X.; Xie, M.; Cheng, Q. Fabrication of  $\text{Cu}_2\text{O}/\text{TiO}_2$  nano-tube arrays photoelectrode and its enhanced photoelectrocatalytic performance for degradation of 2,4,6-trichlorophenol. *J. Ind. Eng. Chem.* **2018**, *57*, 181–187. [\[CrossRef\]](#)
104. Wang, W.K.; Zhu, W.; Mao, L.; Zhang, J.; Zhou, Z.; Zhao, G. Two-dimensional  $\text{TiO}_2\text{-g-C}_3\text{N}_4$  with both  $\text{Ti}[\text{sbnd}]\text{N}$  and  $\text{C}[\text{sbnd}]\text{O}$  bridges with excellent conductivity for synergistic photoelectrocatalytic degradation of bisphenol A. *J. Colloid Interface Sci.* **2019**, *557*, 227–235. [\[CrossRef\]](#) [\[PubMed\]](#)

**Disclaimer/Publisher's Note:** The statements, opinions and data contained in all publications are solely those of the individual author(s) and contributor(s) and not of MDPI and/or the editor(s). MDPI and/or the editor(s) disclaim responsibility for any injury to people or property resulting from any ideas, methods, instructions or products referred to in the content.